This thesis is submitted in partial fulfilment of the requirements for the degree of Master of Science in Medical Biology

Voxel dimension optimization for probabilistic tractography in rat brain using 7T scanner

Jan Kurzawski

University of Bergen, Department of Biomedicine

University of Eastern Finland, A.I. Virtanen Institute for Molecular Sciences

Arvid Lundervold, Professor

Alejandra Sierra Lopez, PhD

Raimo Salo, MSc

Kuopio, 06.2015

Acknowledgements

Firstly I would like to express my gratitude for Professor Arvid Lundervold for introducing me to the field of MRI, encouraging me to apply for a master's programme at University of Bergen and becoming my supervisor for the final project. I had a chance to develop my knowledge in one of the most interesting fields of physics. I would also like to thank all my supervisors from A.I Virtanen Institute at University of Eastern Finland for support and answering complicated questions. I would like to thank Professor Olli Grohn for accepting me as a master student and allowing me to join a multidisciplinary research group. It was a great pleasure to be involved in the work done at AIVI.

I would like to thank Raimo Salo for helping me with all software related problems, introducing me to "makefiles" and for letting me use his experience in writing bash scripts. I would also like to thank Alejandra Sierra Lopez for introducing me to the world of microscopy and histology.

Finally I would like to thank my fellow co-workers Lauri, Eppu, Kaveh and Karthik for a great atmosphere in the lab and friendly collaboration.

TABLE OF CONTENTS

LIST OF FIGURES

LIST OF ABBREVIATIONS

NMR	*Nuclear Magnetic Resonance*
ADC	*Apparent Diffusion Coefficient*
DTI	*Diffusion Tensor Imaging*
GE	*Gradient Echo*
SE	*Spin Echo*
WM	*White Matter*
GM	*Grey Matter*
Vs	*Voxel size*
Vx,	*Voxel dimension in x*
Vy	*Voxel dimension in y*
ST	*Slice Thickness*
NPe	*Number of phase encoding steps*
NPe_2	*Number of second phase encoding steps*
NFe	*Number of frequency encoding steps*
TR	*Repetition Time*
TE	*Echo Time*
NEX	*Number of excitations*
FOVx	*Field of view in x direction*
FOVy	*Field of view in y direction*
FOVz	*Field of view in z direction*

Summary

Brain connectivity is an increasingly important research field within neuroscience. Using MRI technology it is now possible to measure diffusion to approximate the location of anatomical tracts in the brain or correlate certain brain activity to obtain information about functional connectivity (Jirsa & McIntosh, 2007). However, those techniques face many challenges and the results obtained are only an approximation of the truth. Processing of such data includes many complicated steps and the final statistical result is sensitive to the quality of acquired images. Diffusion tensor Imaging (DTI) is a technique which is plagued with inherently low signal to noise ratio (SNR) due to e.g. T2* effects and eddy currents. T2* effects are a combination of both magnetic field inhomogeneites and susceptibility artifacts (Westbrook & Kaut, 1993). By optimizing the sequence parameters the overall quality of the acquired images can be improved, enabling better quantification. Thus, choosing a proper MRI sequence is crucial while performing an experiment. An optimization step for selecting a proper voxel dimension for DTI is introduced in the thesis. The project consists of image acquisition, statistical analysis and visual comparison between tracking results. Nine different 2D sequences and two 3D sequences were tested with different resolution varying in Field of view (FOV), Number of phase and frequency encoding steps, b value and number of averages. Finally a slice thickness of 0.4 mm was chosen, FOV of 12.8 mm and a matrix 64x64 resulting in 2 h 8 min of scanning time.. All of the experiments were performed on rat brain using 7T preclinical scanner, a similar protocol may be used for optimizing MRI sequences in human studies.

Keywords: Diffusion Tensor Imaging, preclinical imaging, optimization, MRI sequences.

1 Introduction

In this section, physics involved in MRI, DTI and theoretical background for the project is briefly discussed.

1.1 MRI physics

MRI was initially named Nuclear Magnetic Resonance (NMR) after Felix Bloch in 1946, He discovered that the atomic nucleus behaved as a magnet. However, the name was changed to MRI as it was believed that the word 'nuclear' would not be widely accepted by the general public. In 1952 Felix Bloch and Edward Purcell received a Nobel Prize in Physics 'for their development of new methods for nuclear magnetic precision measurements and discoveries in connection therewith'.

Basically, an atom consists of a centrally located nucleus containing positively charged protons and neutrons that have no charge. The nucleus is surrounded by an electron cloud consisting of negatively charged electrons. The number of protons in the nucleus is also known as the atomic number whereas the number of protons and neutrons are together known as the atomic mass number.

An atom with an odd atomic number has an angular momentum causing the positively charged nuclei to rotate or spin around its axis. This spin produces a magnetic field and as a result, the atomic nuclei behave like a tiny bar magnet.

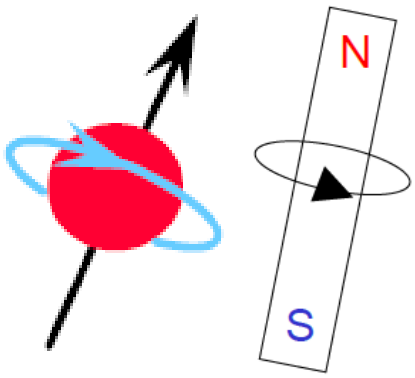

Figure 1-1 Atomic Spin (Blink, 2004).

One of the atoms that exhibit this property is hydrogen. It is the most commonly used element for MRI (Filler, 2009). In a molecule, hydrogen atoms behave like a bunch of bar magnets spinning around their axis in a random direction. This causes their magnetic forces to cancel each other and the resulting net magnetization to be zero.

When an external magnetic field B0 is applied, nuclear spins are starting to align either in parallel or anti-parallel to the field. More energy is needed to align anti-parallel that is why most of the protons are aligned in parallel to the field. The difference between the aligned protons is defined by the strength of magnetic field (McRobbie, 2007).

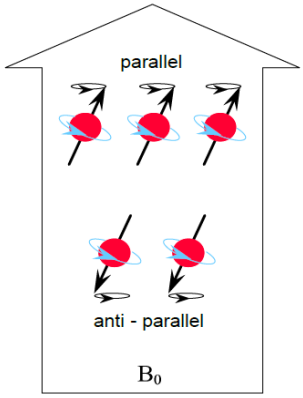

Figure 1-2 Energy states of an atom (Blink, 2004).

After the alignment spins wobble around the axis in which B0 field is applied. This phenomenon is called precession.

Figure 1-3 Atomic precession (Blink, 2004).

The resonance frequency (Larmor frequency) or the frequency of precession is defined by the strength of the external magnetic field and gyromagnetic ratio (McRobbie, 2007).

$$\omega 0 = \gamma * B0$$

Where $\omega 0$ is Larmor frequency [Hz], γ- gyromagnetic ratio [Mhz/T], B0– strength of magnetic field [T]. Magnetic vector of spinning hydrogen protons consist of two components: longitudinal and transverse component. The difference between parallel and anti-parallel nuclear spins is responsible for creation of the longitudinal component also known as "longitudinal magnetization- Mz".

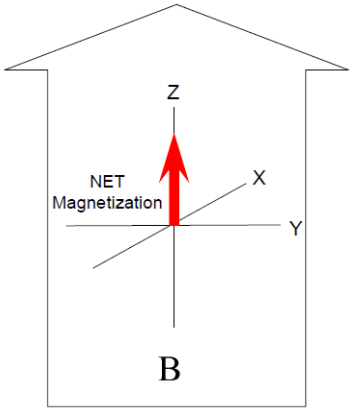

Figure 1-4 Longitudinal magnetization (Blink, 2004).

The second component is created due to the fact that spins are not rotating in phase, thus it is called "transverse magnetization- Mxy" (McRobbie, 2007).

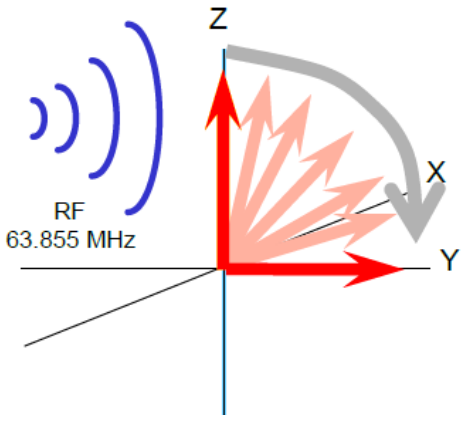

Figure 1-5 Transverse magnetization (Blink, 2004).

Protons, which are precessing in the same frequency, can exchange energy. This phenomenon is called resonance. Magnetic resonance corresponds to the exchange of the energy between the protons and radio frequency pulse. While the scanner applies RF pulse it excites protons, but only the ones, which are spinning in the same frequency as the frequency of the applied pulse. RF pulse excites the protons by energy transfer and puts them into excitation states. When they return to their ground state the electromagnetic energy is released and the scanner receives the signal. This process is known as "relaxation".

In the excitation state proton jumps to the higher energy state (the spins which are aligned parallel, now are aligned anti-parallel), afterwards it releases the energy thus the net magnetization vector is moved to XY plane (McRobbie, 2007). This phenomenon is called "T1 relaxation".

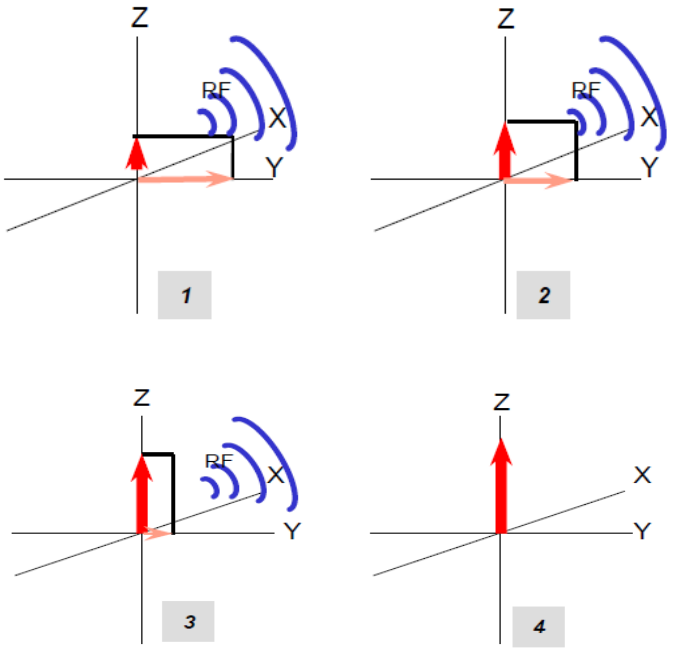

Figure 1-6 T1 relaxation (Blink, 2004).

Just after flipping the net magnetization to XY plane protons are starting to desynchronize and we are losing signal (Filler, 2009). This phenomenon is called "T2 relaxation".

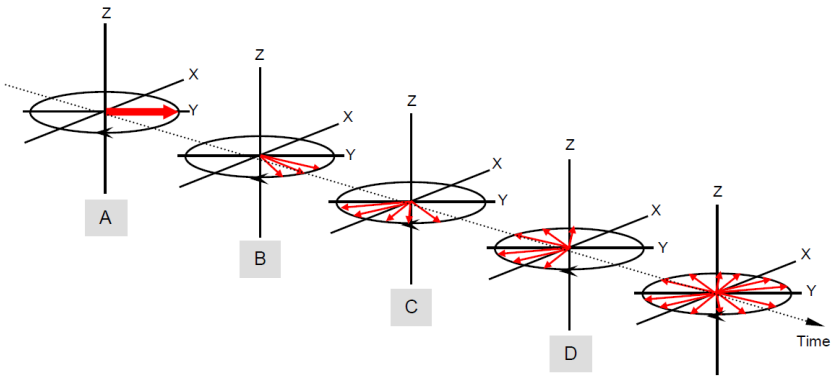

Figure 1-7 T2 relaxation (Blink, 2004).

This is the reason; the 180 degree RF pulse is applied and while the protons are in phase the signal is collected by the detector. This signal decay is known as “free induction decay” (Filler, 2009).

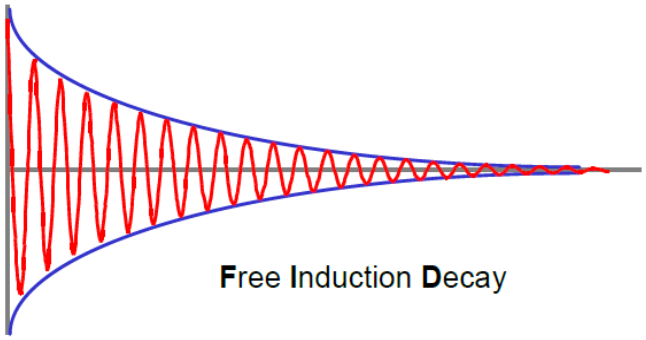

Figure 1-8 MRI signal (Blink, 2004).

By choosing different flip angles (FA) and applying different gradients (to speed up/slow down rephrasing/dephasing in XY plane) different MR sequences are used (Filler, 2009). By changing those parameters different contrasts are collected for different tissues. For example, T2 weighted image will show bright liquids and dark soft tissue (McRobbie, 2007).

To obtain information from where the signal is coming, three gradients are introduced. First gradient is superimposed on B0 in the Z direction and it is called slice selection gradient (GSE). The amount of magnetization is affected by a gradient in linear manner, thus it is possible to predict exact precession frequency of the protons and precisely excite one slice (Filler, 2009). Resonance of protons in surrounding slices will not occur due to their different frequency. Remaining two gradients are applied in X and Y direction named accordingly phase encoding gradient (GPE) and frequency encoding gradient (GFE) (McRobbie, 2007).

1.2 MRI Sequences

1.2.1 Spin Echo

Spin echo sequences use 90° RF pulse to flip the NVM to the transverse plane. After the vector is flipped, due to T2 relaxation spins are starting to dephase and a significant loss of signal is experienced (Bushberg, 1994). To prevent this, 180° pulse is applied. Spins, which were precessing slower, are now ahead and spins precessing faster are now behind (Bushberg, 1994). This phenomenon forces them to come in phase again and produce an echo. Time to echo is a time between application of RF pulse and an echo time (TE). The time between two pulses is known as time to repeat (TR). The resulting signal is called a Spin echo (Bushberg, 1994).

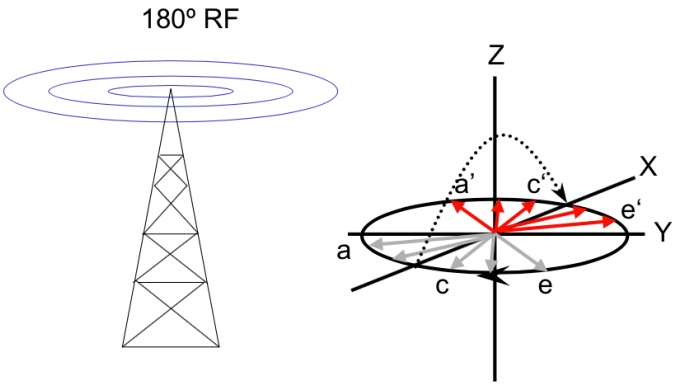

Figure 1-9 Application of 180 degree pulse (Blink, 2004).

The advantages of spin echo are the robustness of the signal and a compensation for local inhomogenities. The disadvantage is high caused by long TR's (Bushberg, 1994).

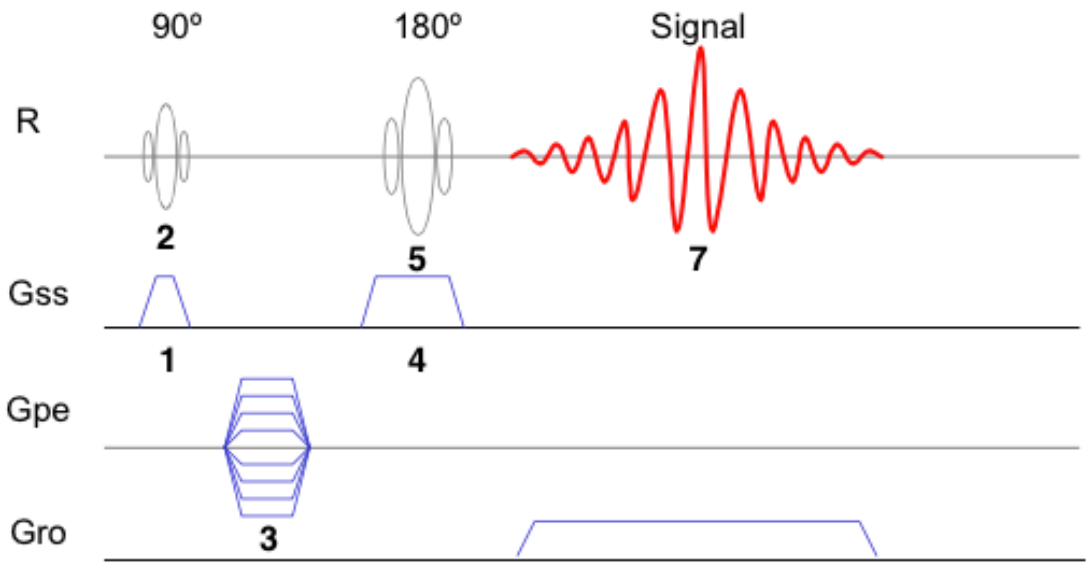

Figure 1-10 Spin Echo sequence (Blink, 2004).

1.2.2 Gradient Echo

Another group of sequences is called gradient echo (GE). While SE is using 180° degree pulse to obtain an echo, GE uses gradients by changing their polarity and affecting the spins (Guy & Ffytche, 2005). They are affected in the same manner as in SE but instead of flipping them by 180 degrees, gradients are fastening the process of dephasing and rephrasing them again to obtain an echo. The amount of magnetization flipped to the transverse plane depends on the Flip angle (FA). The biggest advantage of GE sequence is short time of acquisition achieved by faster dephasing and a possibility of using shorter FA's than 90°. With lower FA's longitudinal relaxation occurs faster (Guy & Ffytche, 2005). The biggest disadvantage is that there is no compensation for magnetic inhomogeneities, therefore GE sequences are sensitive to susceptibility artifacts. While T2* effects are not eliminated T2 decay becomes T2* decay (Guy & Ffytche, 2005).

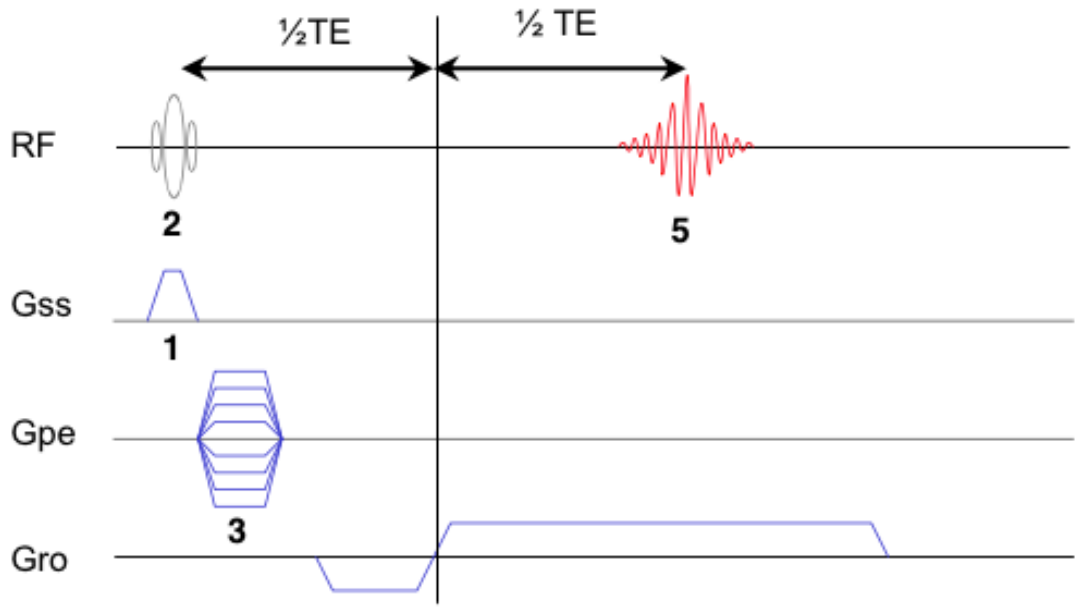

Figure 1-11 Gradient echo sequence (Blink, 2004).

1.3 Diffusion Tensor Imaging

DTI is an MRI technique, which is used to characterize the movement of water molecules (Jones, 2006). The anisotropic behaviour of water molecules within structures of the brain is synthesized in DTI. By introducing a pair of extra gradients to the MRI sequence it is possible to measure the resultant signal attenuation and calculate the apparent diffusion coefficient (ADC) (Jones, 2006). The information from each voxel is transformed into a matrix that characterizes the water molecular diffusion in the tissue and is represented in the form of an ellipsoid. DTI can be used to reveal anatomical changes caused by neurological disorders like Alzheimer's disease, schizophrenia, stroke and multiple sclerosis (Waren et al., 2004).

1.3.1 Diffusion physics

DTI is based on the phenomenon called the "Brownian motion" (Jones, 2006). It's a random movement of the water molecules due to the thermal motion (Mörters et al., 2008). Water molecules are constantly moving and the rate of their movement depends on their kinetic energy and the temperature of the environment (Mörters et al., 2008). In the living organism, the diffusion is not completely random due to the fact that biological tissues have structures (Thibodeau & Patton, 1997). In case of the brain there are vascular walls, myelin around the

axons or cell membranes, which are affecting the diffusion (Thibodeau & Patton, 1997). The amount of the diffusion (diffusion coefficient) can be calculated from Einstein's formula, which states that diffusion depends on the **τ**, which is the time, and **r** which is the displacement (Einstein et al., 2014).

$$D = \frac{1}{6\tau} r^2$$

1.3.2 DTI Physics

In order to perform a DTI experiment additional pair of gradients is used in the MR sequence (Jones, 2006). Their role is to focus and refocus spins in the transverse plane and make the MR signal sensitive to the diffusion of water molecules (Mori & Tournier, 2014). This happens due to the fact that 100% refocusing happens only when the molecules do not change their location between the applications of the gradients. Dephasing gradient marks the signal phase of the water molecules. If diffusion occurs and the location of the molecules is changed, the phase of the moving molecule after rephrasing will be different than the stationary one. As a result diffusion affects the signal intensity in MR image (Mori & Tournier, 2014).

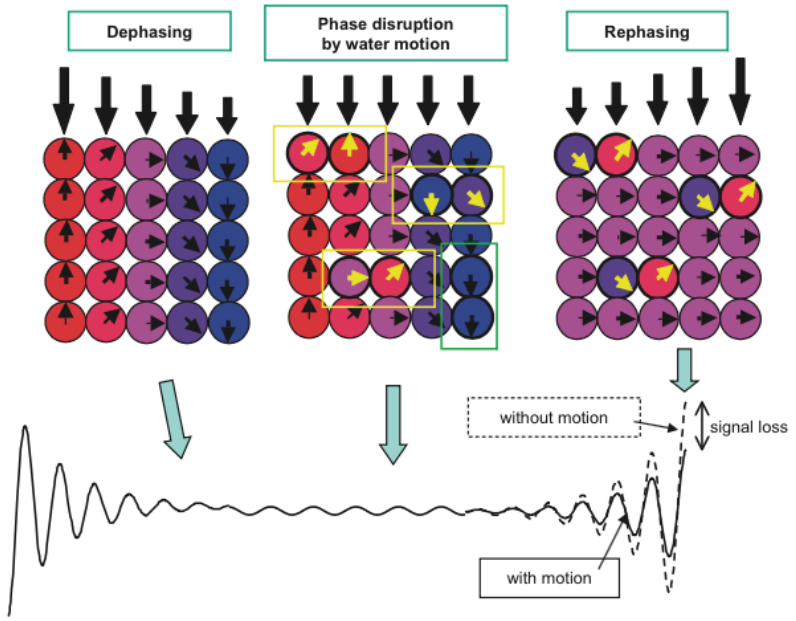

Figure 1-12 Effect of molecular motion onr MR signal intensity (Mori & Tournier, 2014).

While using the gradients in diffusion weighting, certain amount of signal is lost due to T2* effects (Mori & Tournier, 2014). To further avoid signal loss while refocusing the spins usually spin-echo sequences are used and signal decays with T2 constant (Jones, 2006). After the application of the first gradient a 180 degree pulse is used, rephasing the spins (Mori & Tournier, 2014).

The amount of desired diffusion can be modified by the value called the b-value introduced by Bihan et al., 1986. It is a combination of the gradient properties that is used to achieve the diffusion weighting (Mori & Tournier, 2014).

$$b = -\gamma^2 G^2 \delta^2 (\Delta - \frac{\delta}{3})$$

Where γ is a gyromagnetic ratio, G the strength of the gradient, δ the length of the gradient and Δ the application time.

Due to the fact that diffusion can be only measured by the signal loss not only the signal intensity of the weighted image, always a reference image called B0 is acquired (Mori & Tournier, 2014).

$$\frac{\ln(S)}{\ln(S_0)} = -bD$$

S in the equation stands for the signal intensity in the weighted image, S_0 is the signal intensity in the image without weighting and b the b-value.

With different b-values different images are achieved and the higher the b-value is, the more diffusion weighted image is (Jones, 2006).

1.3.3 White matter organization

White matter consists of neurons, which are the main structural element of the nervous system. Their function is to transfer information between different places of the brain (Fields, 2008). Neurons are built of the cell body, the axon and the dendrite (Nicholis, 2012). While dendrites are mostly present in grey matter and are responsible for receiving impulses from other neurons, axons are long “tubes” in the white matter that transmit the electrical impulses away from cell body (Nicholis, 2012). Most axons present in white matter are covered with

myelin sheath. Myelin affects the direction of the diffusion inside the cell due to the presence of physical boundary (Basser, 1995); therefore water diffuses along the axons (Mori & Tournier, 2014). Axons are grouped together to form bigger bundles that are proceeding into one direction. Such groups are called white matter tracts (Mori & Tournier, 2014).

In 1795 Johan Christian Reils created first journal of physiology. His first articles were related to the description of brain structures. By dissecting the brain he revealed main white matter tracts connecting parts of the brain. One of the first discovered connections were direct tracts between occipital and frontal lobe (Jones, 2006). In 1884 Professor Hermann Theodore Meynert published Clinical Treatise on Diseases of the Fore Brain where he classified the white matter bundles into three groups (Meynert, 1968). First group consisted of the fibers starting and terminating in the cortex, second of commissural fibers which were connecting cortex between the hemispheres and the last group which connected parts of the cortex within a hemisphere (Meynert, 1968). Meynert greatly contributed to the findings in neuroanatomy and therefore created a theory of physiological functions (Meynert, 1968).

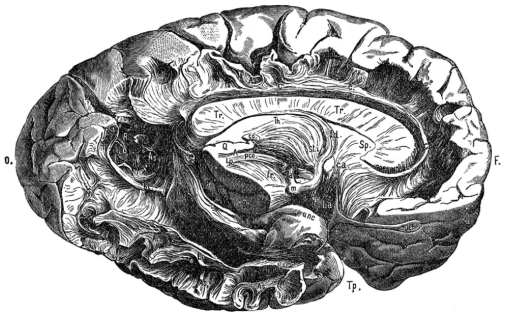

Figure 1-13 Fibers in gross dissection of the medial surface of the human brain (Jones, 2006).

1.3.4 DTI Tractography

To investigate brain fibers in vivo, diffusion tensor imaging tractography was introduced (Basser et al., 2000). Tractography offers a non-invasive imaging technique of myelinated axons by following the diffusion inside them (Basser et al., 2000). By acquiring weighted images in many directions it is possible to estimate main orientation of white matter bundles and therefore distinguish different directions of fibers in the brain (Jones, 2006). DTI assumes that diffusion can be modelled as an ellipsoid and mathematically described by six parameters. – 3 eigenvectors and 3 eigenvalues (Mori & Tournier, 2014). Eigenvalues and

eigenvectors are obtained from diagonalization of the 3x3 tensor matrix obtained from diffusion measurements (Jones, 2006). To fit the tensor at least 6 different weighted independent measurements are necessary in different directions. Acquiring more than 6 images improves the tensor fitting and enhances the information about tensor orientation (Mori & Tournier, 2014).

A constant describing the shape of the ellipsoid is called fractional anisotropy (FA) (Jones, 2006). It is calculated from eigenvalues and eigenvectors of the tensor. Eigenvectors λ_k give the direction of the diffusivity while corresponding eigenvalues $\lambda_j^k$the magnitude (Mori & Tournier, 2014).

$$FA = \sqrt{\frac{1}{2}}\frac{\sqrt{(\lambda_1 - \lambda_2)^2 + (\lambda_2 - \lambda_3)^2 + (\lambda_3 - \lambda_1)^2}}{\sqrt{\lambda_1^2 + \lambda_2^2 + \lambda_3^2}}$$

This type of calculation is performed for every voxel of the image (Basser, 1995). It gives the information about isotropy, showing the behaviour of the diffusion. Other parameters like mean diffusivity (MD), main diffusion direction (V1) may be calculated (Gulani et al., 2001). In water FA value is close to 0 because the diffusion is free and it is not restricted, however when FA gets close to 1 it means that diffusion occurs mainly in one direction (Jones, 2006).

DTI results are often presented in a 2D manner as a colormap showing main the diffusion direction in every pixel/voxel (Mori & Tournier, 2014). It is presented by using three major colors (red, blue, green) corresponding to the orientation of the diffusion (Jones, 2006). Fibers in red are usually represented from right to left, in blue anterior to posterior and in green superior to inferior. The colormap represents main diffusion directions in the brain (Mori & Tournier, 2014).

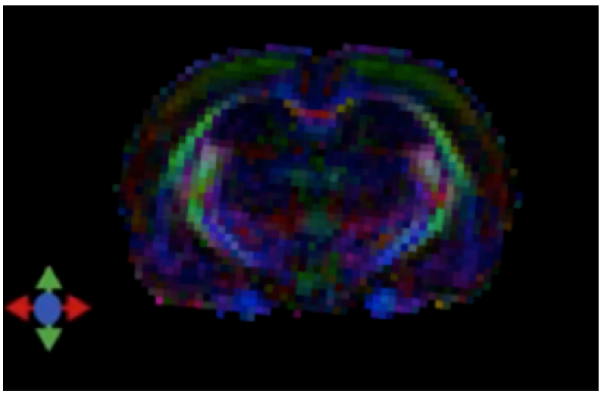

Figure 1-14 Colormap of the rat brain. Colormap was created (by the author) by multiplying FA map and V1 map.

DEC maps are the most common way of representing 2D DTI data, however it does not provide complete information regarding the 3D shape of the tracts.

For this reason, 3D reconstruction of diffusion data is performed that enables identification and mapping of individual white matter trajectories. This technique is known as "tractography" (Basser et al., 2000). There are many ways to perform tractography where the simplest one is called voxel-linking (Mori & Tournier, 2014). In this technique, connectivity information is obtained using a probabilistic algorithm to obtain fiber orientation estimates from each voxel with neighbouring voxels. As the algorithm traverses from one voxel to another, it uses this connectivity information to generate a desired number of streamlines i.e. fiber tracts (Mori & Tournier, 2014).

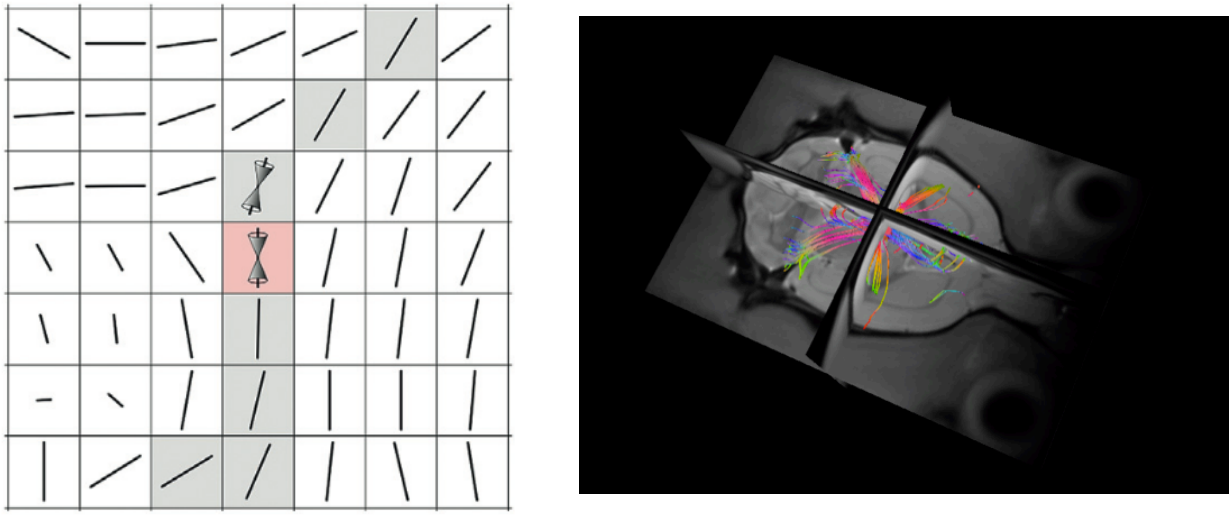

Figure 1-15 Voxel linking and Corpus Callosum tracts. Scheme on the left present voxel linking (fiber tracking) technique. On the right Corpus Callosum tracts reconstucted from rat. Image was produced by the author using DSI studio.

2 Aims

The objective of the dissertation is to optimize existing imaging sequences and parameters for probabilistic tractography on high-field magnets for rat brain. Parameters such as the repetition time (TR), number of excitations (NEX), number of directions for diffusion weighted images, b-value and signal to noise ratio (SNR) are explored. Parameters will be chosen to allow the in-vivo experiment have a maximum scan time of 2,5h on a 7T scanner. The special focus of the thesis is the effect of the voxel size and dimensionality on SNR in probabilistic DTI fiber tracking. The project aims to establish a DTI sequence for in-vivo studies that will give comparable results to histological examination and may be used as a reference. The project comprises image acquisition, statistical analysis and a comparison between data acquired with different parameters.

3 Materials and Methods

Following chapter describes all steps undertaken to complete the project. It includes description of equipment, animal handling, software used for analysis. Project is carried out at A.I.Virtanen Institute, University of Eastern Finland under the supervision of Professor Arvid Lundervold (UiB), Alejandra Sierra Lopez, PhD and Raimo Salo, MSc.

3.1 Equipment

All MR images were acquired on a Bruker scanner 7 T, 16 cm diameter bore magnet, PharmaScan© (Bruker BioSpin MRI GmbH, Ettlingen, German). A Volume RF-coil (diameter 70 mm, Rapid Biomedical GmbH, Rimpar, Germany) was used as a transmitter and quadrature surface coils as a receiver. MR station was equipped with Paravision 5.1 software (Bruker BioSpin MRI GmbH, Ettlingen, German). Temperature was monitored by a fiber optic rectal probe. Breathing rate was monitored by placing a pneumatic pillow sensor pad under the abdomen of the animal. Both temperature and respiration were monitored by a small animal MR-Compatible, Model 1030 monitoring system (Small Animals Instruments Inc).

3.2 Animals

9 adults wistar rats were used (~400 grams) for the MRI experiment. The animal facilities have 12 h light/12 h dark cycle (7:00-19:00) with constant temperature (22±1°C) and humidity (50–60 %). Animals had free access to food and water. All animal procedures were approved by the Animal Care and Use Committee of the Provincial Government of Southern Finland and conducted in accordance with the guidelines set by the European Community Council Directives 86/609/EEC.

3.3 Anaesthetic procedure

Anesthetic procedure begins with checking the levels of gases obligatory for anesthesia (Isoflurane, Nitrogen and Oxygen). Rat is taken out of the animal cage and placed in the special chamber where gas tubes are connected. Incubation is performed in a special chamber using 5% of Isoflurane, 60% of Oxygen and 40% of Nitrogen. In the time of approximately 5

minutes the rat is anesthetized and pedal reflexes are starting to disappear. Animal may be transferred to the special small animal MRI holder.

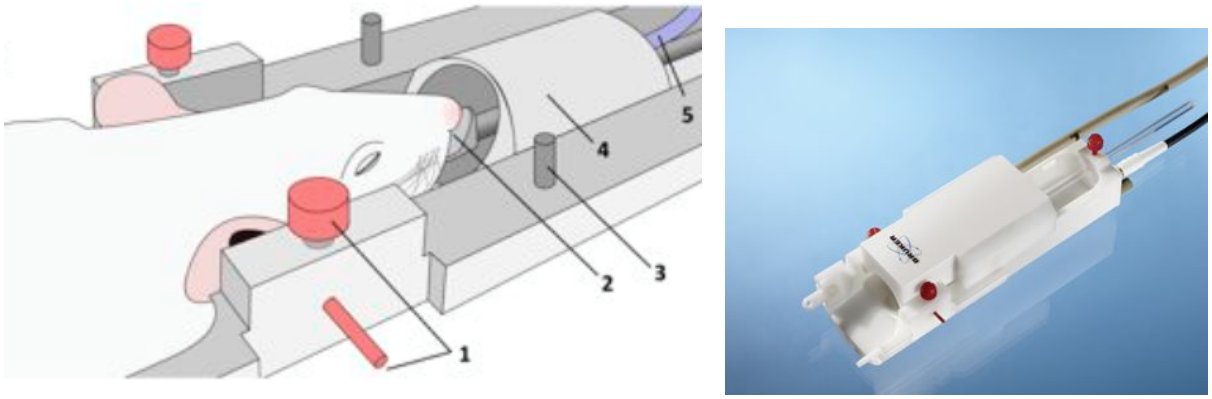

Figure 3-1 Animal holder. 1- Ear pins, 2- Bite bar, 3 – markers for positions, 4- Cover for proper gas flow, 5- Tube supplying the anaesthesia. Animal holder is placed in a manner that is freely movable along the z-axis in the system. By adjusting the position of the holder it is possible to place the rat brain in the isocenter (Kalthoff, 2011).

Animal upper teeth are placed in the bite bar and pins are placed inside both ears to ensure proper positioning and prevent movements during the experiment. Accurate positioning allows appropriate gas flow and effective anaesthesia. In the holder anaesthesia is maintained with 1-1,5% of Isolflurane varying with animal's physiology. The tip of mouse head has to be covered to omit gases spreading away from the system.

3.4 Physiological monitoring and positioning

Monitoring of physiological functions during the MRI experiment is crucial. To maintain accurate level of anaesthesia and prevent the animal from moving and waking up several vital functions are controlled.

3.4.1 Temperature

A rectal probe measures body temperature. Warm water is transferred via the water heating system to prevent from loosing heat. Temperature of water can be adjusted and usually it is set to keep the animal body temperature between 35.9-37.5ºC.

3.4.2 Respiration

A pad sensor is placed under the animal's body, reacting on the contractions of the thorax. Based on the movement of the abdomen the signal is read and transformed into electronic readout. The respiratory rate is measured in BMP (breath per minute) and it is maintained between 60-90 BMP.

3.4.3 Hardware

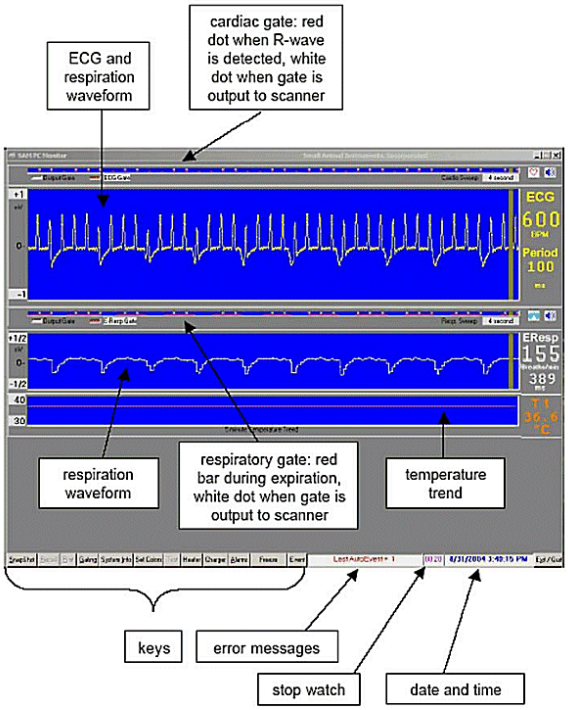

Figure 3-2 Screenshot from monitoring software (Bruker). Parameters such as breathing rate, heart rate and temperature can be monitored.

Monitoring was performed with Small Animals equipment (Small Animal Instruments Inc., Stony Brook, NY, USA). Sensors were connected to the readout instrument and data was transformed to the PC in the operator room.

3.4.4 Positioning

Animal is transferred to the animal holder and placed in the prone position. Upper teeth are placed in the bite bar and earplugs are moved inside the ears. The respiration pad is placed under the animal. The rectal probe is inserted. After the breathing rate and temperature is

registered on the monitor the MRI animal holder may be placed inside the magnet bore and the experiment may begin.

3.4.5 Withdrawal from anaesthesia

After the experiment all sensors and probes are removed. The isoflurane is on until the animal is completely removed from the holder. The animal is transformed to its cage and left with the access to oxygen. In approximately 5 minutes the breathing rate increases significantly and animal starts to move again. Animal should be monitored for couple more minutes and can be taken back to the animal room.

3.5 MR Imaging

To obtain the first MRI image and check if the rat is positioned properly a pilot scan is performed. It contains one slice from each plane (axial, horizontal, sagittal).

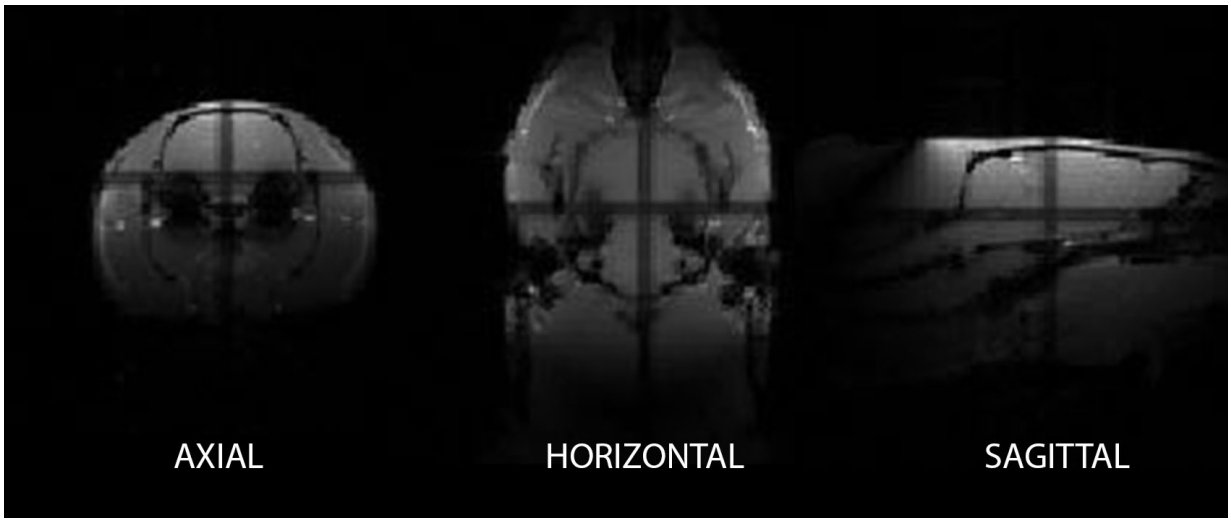

Figure 3-3 Tripilot. Acquistion of tripilot ensures proper positioning in the scanner. Looking at different planes enables proper judgement.

To further ensure that the positioning is proper a tripilot with 14 slices is acquired. While going through axial slices it is easy to see if the brain is in the correct position and if it is not tilted or rotated. Acquiring more slices also improves the judgment on the symmetry of the brain, since it is possible that the brain may be twisted. As EPI is plagued with magnetic filed inhomogeneities (Westbrook & Kaut, 1993) there is a need to correct for the field distortions. A field map is acquired for this purpose and it is registered to the image. Field map is the evolution of the phase of two images with different echo times (Brown et al., 2014). In

Paravision 5.1 a method of acquiring local shim map is used (Bruker).

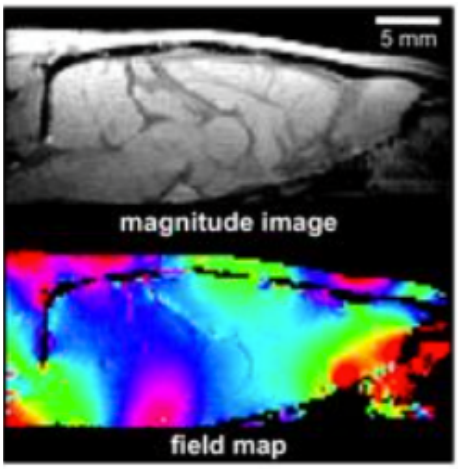

Figure 3-4 Fieldmap acquired with Paravision 5.1 software (Bruker). Colored field map shows the behaviour of local magnetic inhomogneities.

3.5.1 Diffusion data acquisition

This chapter explains a design of the project. It introduces a step-by-step procedure in which DTI sequences were tested.

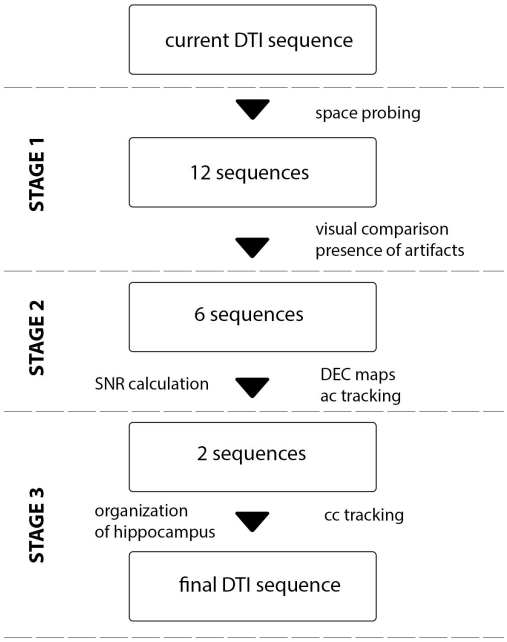

Figure 3-5 Design of the project. Project consisted of 3 stages. After each of them several sequences were discarded.

Project was divided into 3 stages. In the first stage MRI sequences with different parameters were checked. Results were visually assessed for the presence of artefacts. Second stage included tensor fitting, DEC maps comparison and calculation of SNR while in the last stage tractography results and anatomical organization were studied and judged by rat anatomist.

3.5.2 First stage of the experiment

Vx (mm)	Vy (mm)	ST (mm)	TR (ms)	NEX	Slices	Time (min)
0.22	0.22	0.5	2500	14	14	112
0.22	0.22	0.5	4000	10	28	128
0.3	0.3	0.3	4000	4	28	51
0.3	0.3	0.3	4000	10	28	128
0.25	0.25	0.35	4000	10	28	128
0.2	0.2	0.4	4000	10	28	128
0.4	0.4	0.4	4000	10	28	128
0.25	0.25	0.5	4000	10	28	128
0.15	0.15	0.3	4000	10	28	128

Table 3-1 2D sequences tested during the first stage of the experiment.

Vx (mm)	Vy (mm)	Vz (mm)	TR (ms)	NEX	Time (min)
0.22	0.22	0.22	1000	1	194
0.3	0.3	0.3	1000	1	128

Table 3-2 3D sequences tested during the first stage of the experiment.

3.5.3 Second stage of the experiment

In the second stage 6 sequences were examined. SNR was calculated, DEC maps were compared and fiber tracking was performed.

Vx (mm)	Vy (mm)	ST (mm)	TR (ms)	NEX	Slices	Time (min)
0.22	0.22	0.5	2500	14	14	112
0.22	0.22	0.5	4000	10	28	128
0.3	0.3	0.3	4000	4	28	51
0.3	0.3	0.3	4000	10	28	128
0.25	0.25	0.35	4000	10	28	128
0.2	0.2	0.4	4000	10	28	128
0.4	0.4	0.4	4000	10	28	128
0.25	0.25	0.5	4000	10	28	128
0.15	0.15	0.3	4000	10	28	128

Table 3-3 2D sequences tested during the experiment. Sequences marked green were selected for further evalutaion.

Vx (mm)	Vy (mm)	Vz (mm)	TR (ms)	NEX	Time (min)
0.22	0.22	0.22	1000	1	194
0.3	0.3	0.3	1000	1	194

Table 3-4 3D sequences tested during the experiment. Sequences marked green were further evaluated.

3.5.4 Third stage of the experiment

In the last stage of the experiment two selected sequences were finally evaluated

Resolution:

- 2D 0.2 mm x 0.2 mm x 0.4 mm
- 2D 0.15 mm x 0.15 mm x 0.3 mm

3.6 Software

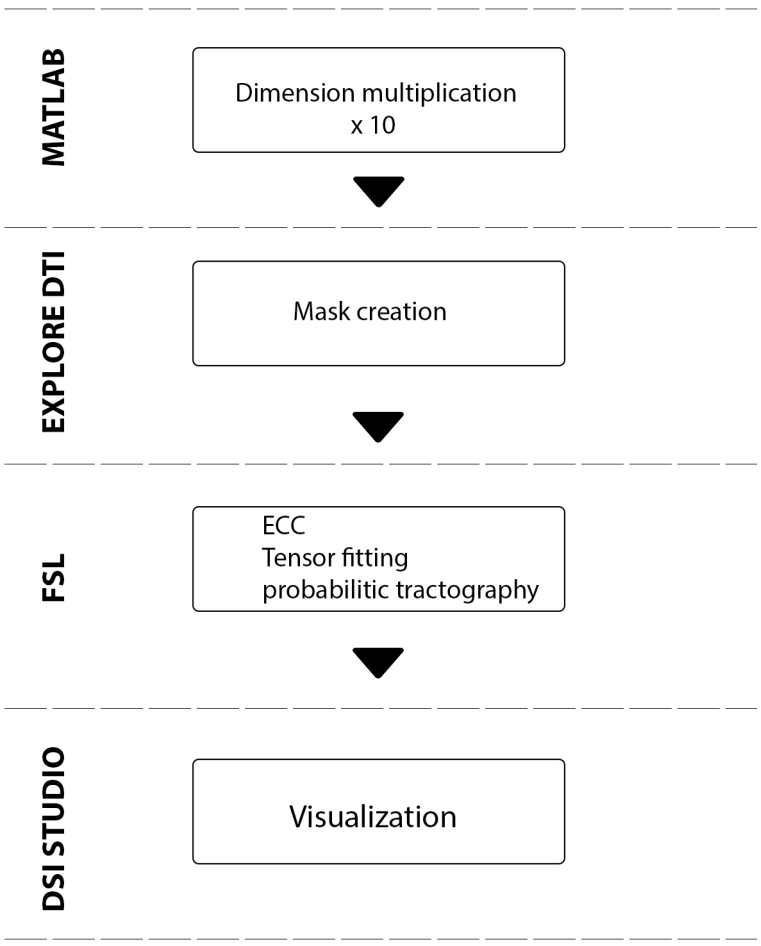

Figure 3-6 Software used during the project.

Data was reconstructed from the scanner using the in-home made MATLAB (mathworks) script and AEDES software (aedes) to make it accessible by other programs. Dimensions of the image were multiplied by a factor of 10 to enable processing of the data by software designed for clincial use. B-vectors and b-values were extracted from the scanner. DTI data is plagued with distortion caused by gradient coils known as “eddy currents". It may cause shearing or squeezing of the image (Brown et al., 2014). The data was compensated for eddy current induced distortions using FSL (Jenkinson et al., 2012). Several types of software were tested for creation of the mask from non-weighted B0 image. Finally ExploreDTI (Leemans et al., 2009) was used as it gave the best results. To fit the tensor and calculate FA maps FSL was used (Jenkinson et al., 2012; FDT). Color coded DEC maps were created in MATLAB (mathworks) by multiplying the FA map and V1 map (main diffusion direction). Deterministic tractography was performed with DSI studio (Yeh et al., 2013) and

probabilistic tractography with bedpostx, probtrackx library package using FSL. (Jenkinson et al., 2012).

3.7 Evaluation criteria

In the first stage of the experiment images with different voxel dimensions were acquired. There were no criteria for choosing the imaging parameters; therefore this stage could be also described as space probing. Sequences were mostly varying in slice thickness and dimensions in X and Y. To keep tractography results most reliable one of the assumptions was to keep slice thickness maximum 2 times higher than X and Y dimensions as tractography gives best results with isotropic voxels. Unfortunately in 2D sequences isotropy can be only achieved with low resolutions. In the sequence that was the starting point for the project only 14 slices were acquired with slice thickness of 500 mm. Due to the fact that it was not covering the whole brain, number of slices was increased to 28 and TR to 4000 to keep number of slices / TR ratio at the same level and not to cause gradient heating. After successful reconstruction of 3D sequences, 2 isotropic sequences were selected.

During the second stage DEC maps were constructed and SNR of B0 images was calculated using following equation.

$$SNR = \frac{\mu sig}{\sigma bg}$$

In the equation above μsig stands for the average signal value and σbg is the standard deviation of the background. ROIs consisted of 9 pixels. Signal from hippocampus was examined. Important evaluation parameter was presence of spatial distortions, which can appear due to magnetic field inhomogeneities (Baldwin et al., 2007). Tractographic reconstruction does not allow presence of any artifacts. Tracts are a geometric object and it would be impossible to asses their shape, direction or orientation. Another criteria was the visibility of hippocampus in the DEC maps. In two 2D isotropic sequences (0.3 mm and 0.4 mm) organization of hippocampus could not be observed, thus those sequences were also discarded. Two remaining sequences were showing promising results with reasonable SNR. Therefore they were chosen for further evaluation.

In the last stage special focus was on the organization of the hippocampus, 2D DEC maps constructed in DSI studio. Fiber tracking on corpus callosum was performed using FSL and connectivity results were judged by histologist.

4 Results

4.1 STAGE 1

Results from the first stage of the experiment are presented below. For each acquisition three volumes were collected. One B0 image and two diffusion weighted images. Images were visually compered. Special focus was on presence of the artifacts. Nine 2D sequences and two 3D sequences were acquired.

Figure 4-1. MRI sequence that was commonly used in the lab for DTI experiments. It was a starting point for the project. Vs = 0,24 mm^3, Vx, Vy = 0,22 mm, ST = 0.5 mm, NPe = 64, NFe = 96, TR = 2500 ms, TE = 30 ms, NEX = 14, Shots = 4, FOVx = 14, FOVy = 21, Time = 112 min, Number of slices = 14, Area covered in Z dimension = 7mm.

Figure 4-2 Sequence with extended number of slices Vs = 0,24 mm^3, Vx, Vy = 0,22 mm, ST = 0.5 mm, NPe = 64, NFe = 96, TR = 4000 ms, TE = 30 ms, NEX = 10, Shots = 4, FOVx = 14, FOVy = 21, Time = 128 min, Number of slices = 28, Area covered in Z dimension = 14mm.

Figure 4-3 First isotropic sequence tested Vs = 0,27 mm^3, Vx, Vy = 0,3 mm, ST = 0.3 mm, NPe = 64, NFe = 96, TR = 4000 ms, TE = 30 ms, NEX = 4, Shots = 4, FOVx = 19,2 FOVy = 28,8, Time = 51,2 min, Number of slices = 28, Area covered in Z dimension = 8,4 mm.

Figure 4-4 Isotropic sequence with higher NEX Vs = 0,27 mm^3, Vx, Vy = 0,3 mm, ST = 0.3 mm, NPe = 64, NFe = 96, TR = 4000 ms, TE = 30 ms, NEX = 10, Shots = 4, FOVx = 19,2 FOVy = 28,8, Time = 128 min, Number of slices = 28, Area covered in Z dimension = 8,4 mm.

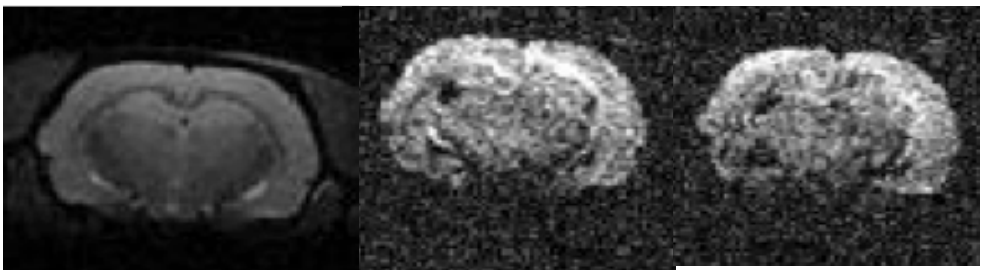

Figure 4-5 Higher resolution 2D sequence Vs = 0,22 mm^3, Vx, Vy = 0,25 mm, ST = 0.35 mm, NPe = 96, NFe = 96, TR = 4000 ms, TE = 30 ms, NEX = 10, Shots = 4, FOVx = 24 FOVy = 24, Time = 128 min, Number of slices = 28, Area covered in Z dimension = 9,8 mm.

Figure 4-6 Sequence with ST = 2 x Vx, Vy Vs = 0,16 mm^3, Vx, Vy = 0,2 mm, ST = 0.4 mm, NPe = 64, NFe = 64, TR = 4000 ms, TE = 30 ms, NEX = 10, Shots = 4, FOVx = 12,8 FOVy = 12,8, Time = 128 min, Number of slices = 28, Area covered in Z dimension = 11,2 mm.

Figure 4-7 Second isotropic sequence Vs = 0,64 mm^3, Vx, Vy = 0,4 mm, ST = 0.4 mm, NPe = 64, NFe = 64, TR = 4000 ms, TE = 30 ms, NEX = 10, Shots = 4, FOVx = 12,8, FOVy = 12,8, Time = 128 min, Number of slices = 28, Area covered in Z dimension = 11,2 mm.

Figure 4-8 Second sequence with ST= 2 x Vx,Vy Vs = 0,31 mm^3, Vx, Vy = 0,25 mm, ST = 0.5 mm, NPe = 64, NFe = 96, TR = 4000 ms, TE = 30 ms, NEX = 10, Shots = 4, FOVx = 16, FOVy = 24, Time = 128 min, Number of slices = 28, Area covered in Z dimension = 11,2 mm

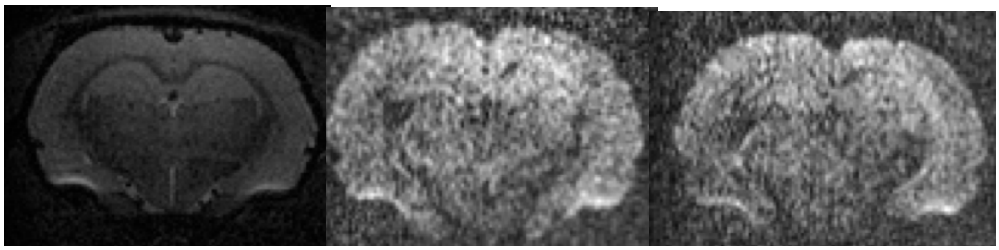

Figure 4-9 Hi-res sequence Vs = 0,06 mm^3, Vx, Vy = 0,15 mm, ST = 0.3 mm, NPe = 64, NFe = 96, TR = 4000 ms, TE = 30 ms, NEX = 10, Shots = 4, FOVx = 16, FOVy = 24, Time = 128 min, Number of slices = 28, Area covered in Z dimension = 11,2 mm

Figure 4-10 First 3D isotropic sequence Vs = 0,027 mm^3, Vx, Vy = 0,3 mm, Vz = 0.3 mm, NPe = 80, NPe_2 = 64 , NPe = 128, TR = 1000 ms, TE = 45 ms, NEX = 1, Shots = 4, FOVx = 16, FOVy = 25,6, FOVz = 1,28 Time = 194 min.

Figure 4-11 Second 3D isotropic sequence Vs = 0,08 mm^3, Vx, Vy = 0,2 mm, Vz = 0.2 mm, NPe = 80, NPe_2 = 64 , NPe = 128, TR = 1000 ms, TE = 45 ms, NEX = 1, Shots = 4, FOVx = 16, FOVy = 25,6, FOVz = 1,28 Time = 194 min.

4.2 STAGE 2

For the second stage of the experiment five 2D sequences from the first stage were chosen and two 3D sequences. The main aim of this stage was to calculate SNR of the images, compare color-coded maps and perform probabilistic fiber tracking. The structure that was used as an origin for tracking was Anterior Commissure (AC).

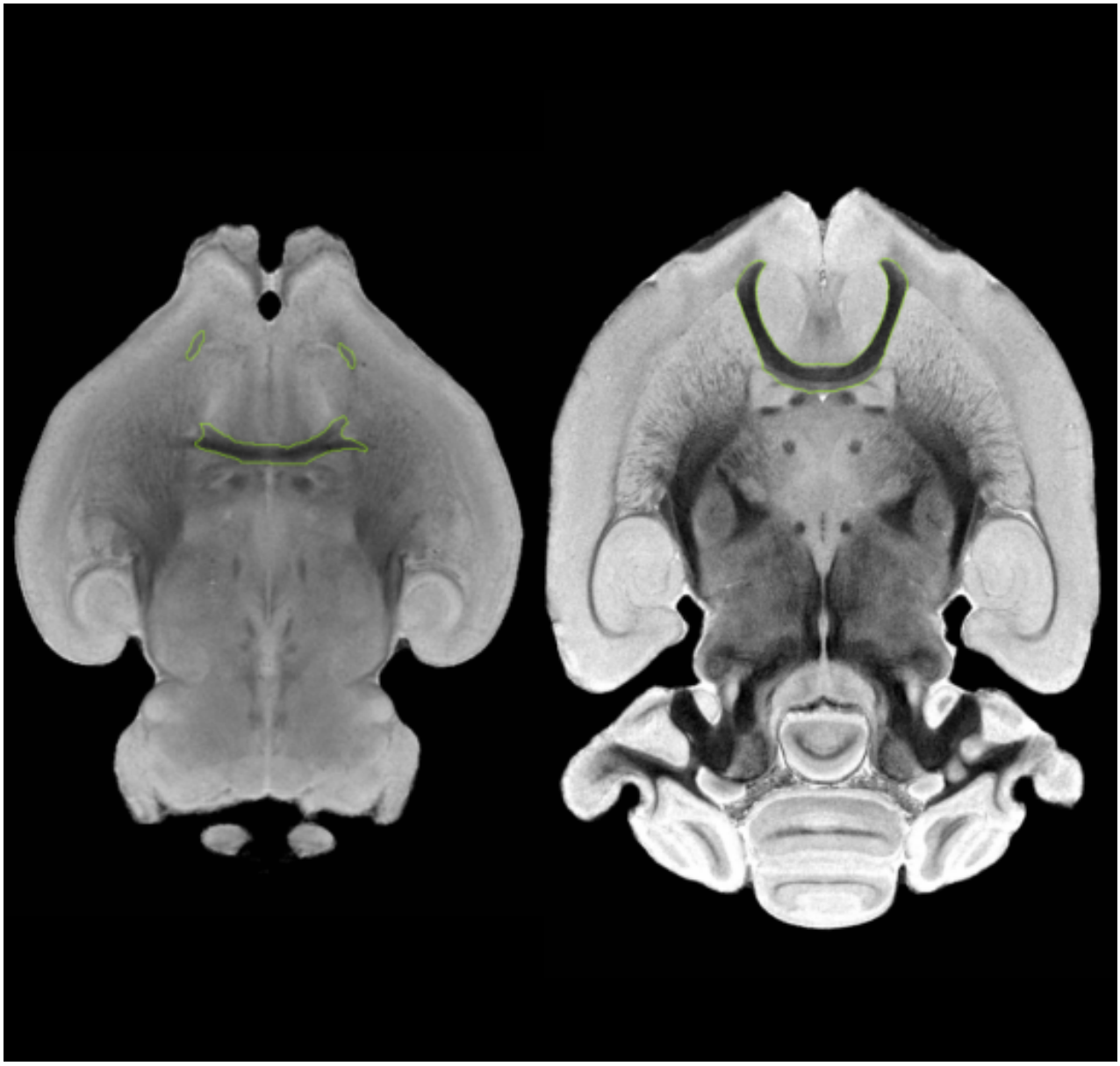

Figure 4-12 Horizontal view on anterior commissure in rat brain. The structure is outlined with green color (Neurolex.org).

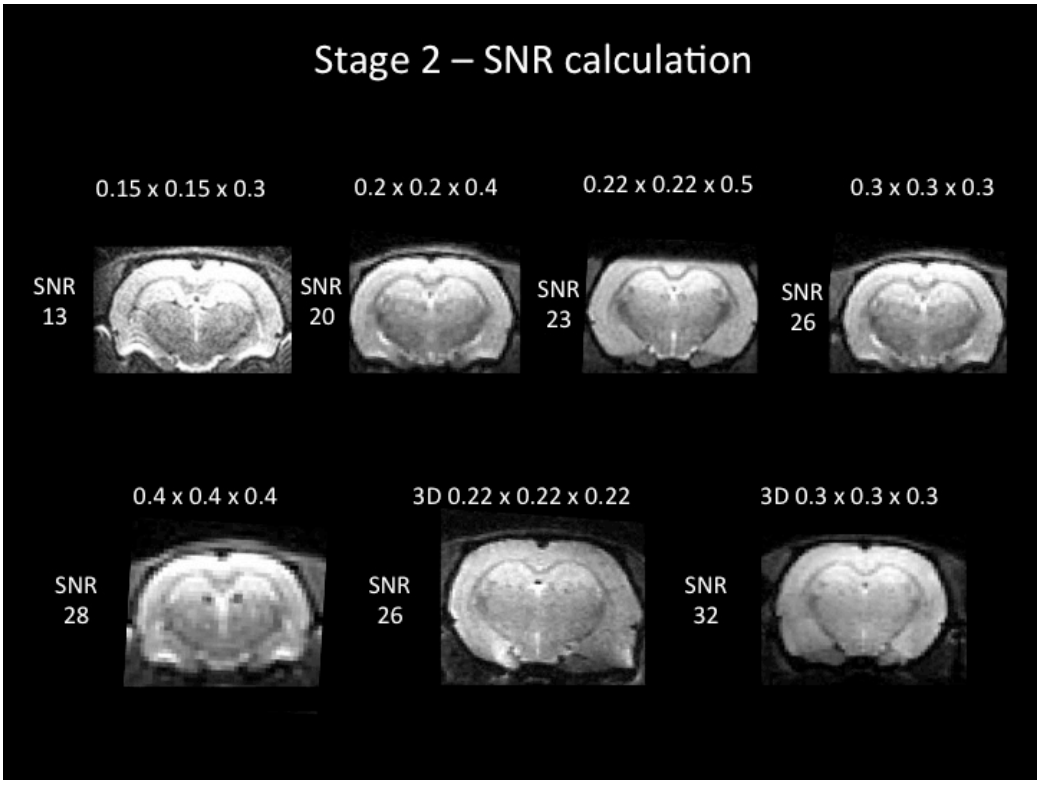

Figure 4-13 Calculation of SNR on B0 maps. Decreasing the resolution improves the SNR. It is caused by Increasing the FOV and decreasing the size of the matrix. Resolution measured in mm.

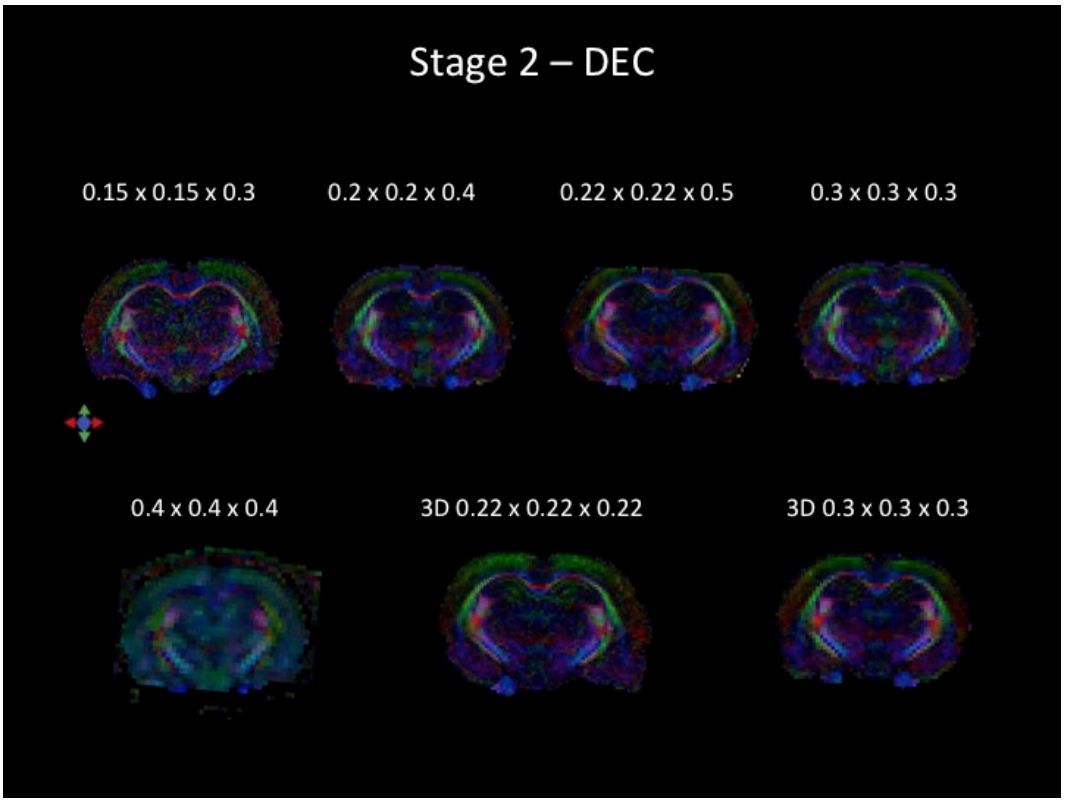

Figure 4-14 Calculation of DEC maps of tested sequences. Maps present that with higher resolution general detail of the image improves. Resolution measured in mm.

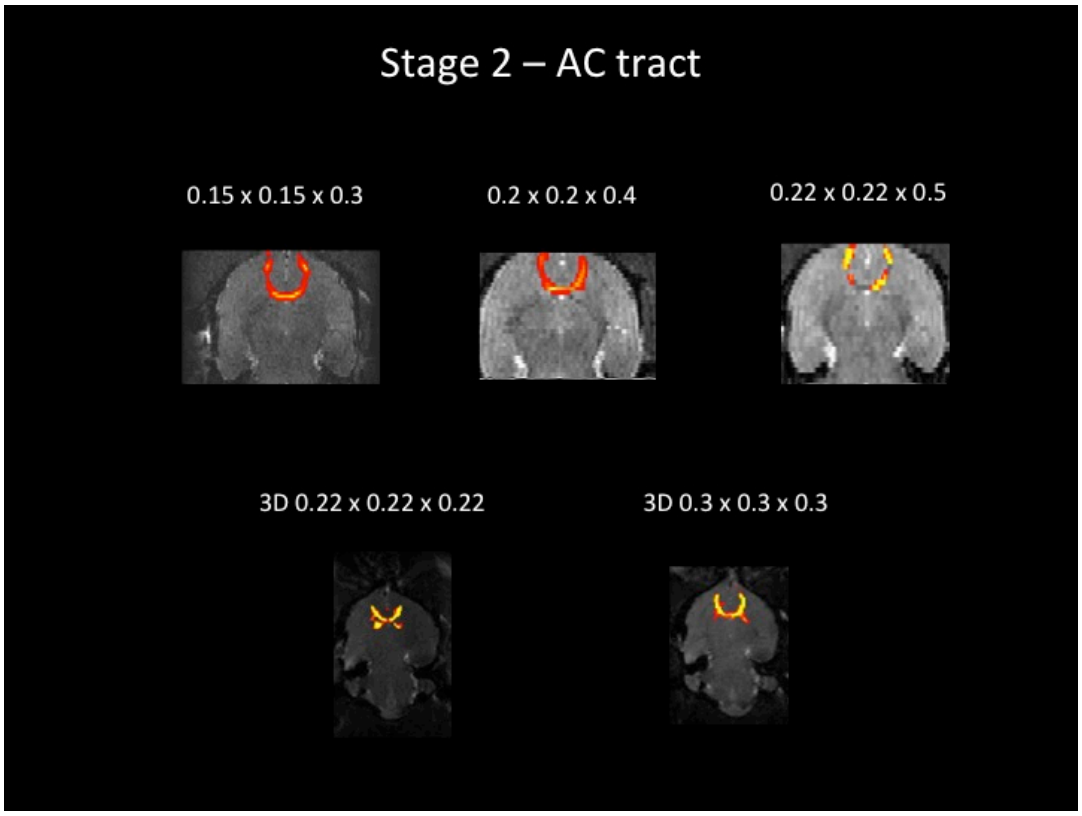

Figure 4-15 Probabilistic fiber tracking on Anterior Commissure. Anterior commissure was selected as a mask for fiber tracking. Tractography was performed using FSL software and FDT toolbox. Resolution measured in mm.

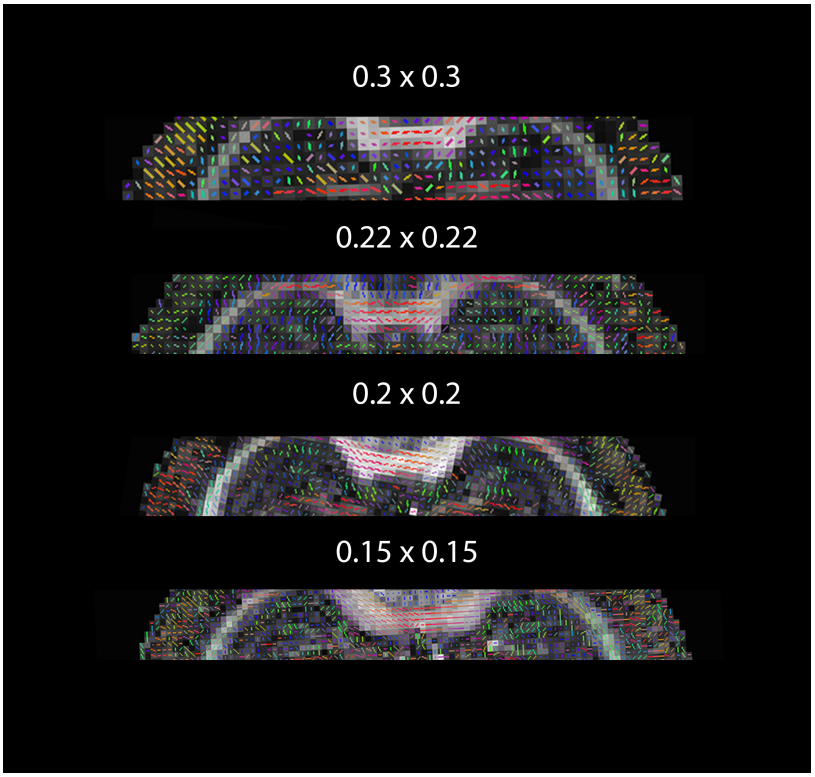

Figure 4-16 Organization of the hippocampus. Figure shows how increaseing the resolution affects the visiblitiy of the hippocampus. Resolution measured in mm.

4.3 STAGE 3

Main aim of the third stage of the experiment was to repeat the tracking procedure on a bigger structure. Main question was if low SNR (~13) allows a proper reconstruction of the tracts. At this point tractography was performed on Corpus Callosum, which should results in high connectivity (Preti et al., 2001)

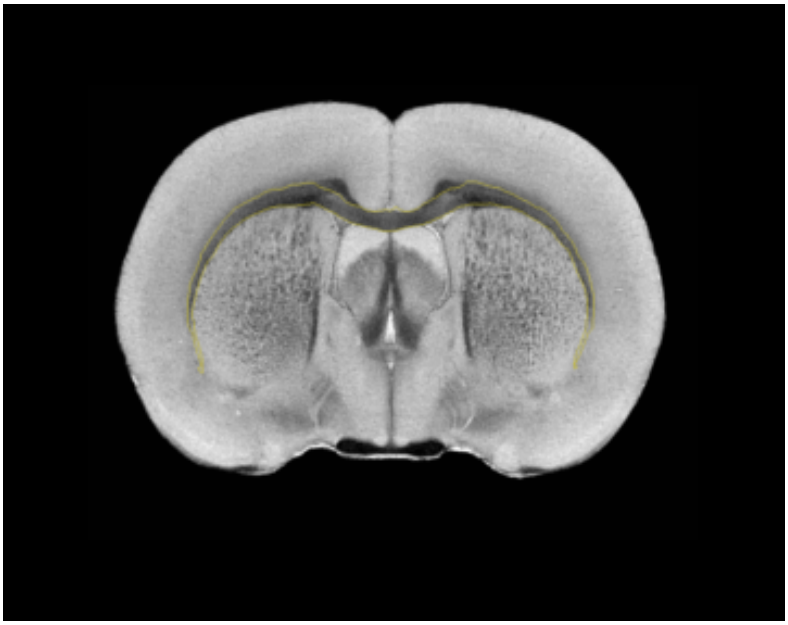

Figure 4-17 Corpus callosum in rat brain outlined with yellow color (Neurolex.org).

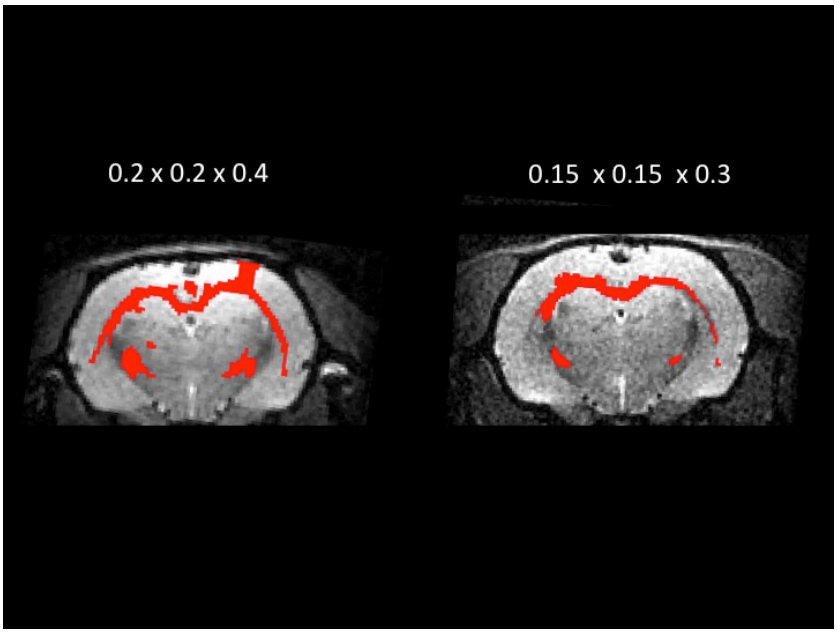

Figure 4-18 Corpus callosum tracts. Results obtained from probabilisitc tractography. Resolution measured in mm.

5 Discussion

5.1 Introduction to the discussion

DTI data is plagued with inherently low SNR (Moseley et al., 2000; Jones & Basser, 2004). Performing and optimization procedure may improve the overall quality of the data and cause better quantification of the results. The aim of the thesis was to explore the effect of several imaging parameters on SNR. Special focus was on voxel dimension. Imaging sequence that was commonly used for DTI experiments in AI. Virtanen institute was used as a starting point for the project.

In the discussion the strengths and weaknesses of the applied methods will be reported in the first part. In the second part, results and future opportunities will be described.

5.2 Strengths and limitations

5.2.1 Project design

The project was designed in a manner that several validation methods are introduced and applied in succession, accompanying the different stages of the project. In the first step images were assessed based on the visual impression and presence of artifacts. In the second step, SNR calculation and tractography was introduced. While in the last step organization of hippocampus was added as judging criteria. This ensured proper evaluation of tested sequences, as it was harder to decide about the quality of the images, therefore more sophisticated methods were necessary. To improve the validation of the project, measurement could be repeated. Unfortunately due to long scanning time and a number of subject included it was not possible.

5.2.2 Animal model

All animals were held in 12 h light/12 h dark cycle (7:00-19:00) with constant temperature (22±1°C) and humidity (50–60 %). Animals were approximately of the same size and age with access to food and water. Animal handling procedures were standardized with the exception of the anesthesia levels used during the scans. Level of isoflurane was set in accordance to the animal physiology (breathing rate and temperature) during the experiment.

Isoflurane is not the most stable anesthetic; therefore it was adjusted during the experiment to keep the parameters at the same level. Experiments on live animals always introduce differences, which cannot be avoided; fortunately they should not influence the quality of the images.

5.2.3 MR imaging

All animals underwent same procedure for an MRI scan. Proper positioning inside the scanner is crucial for the experiment; therefore special marks were made on the animal holder. It is also necessary to assure proper placement of the rat head. For every rat same set of ear pins was used. Each experiment lasted for 2,5 h (including preparation) and it is necessary to ensure that animals are well anaesthetized and they are not moving while being inside the scanner. If any movement was detected, scans were repeated.

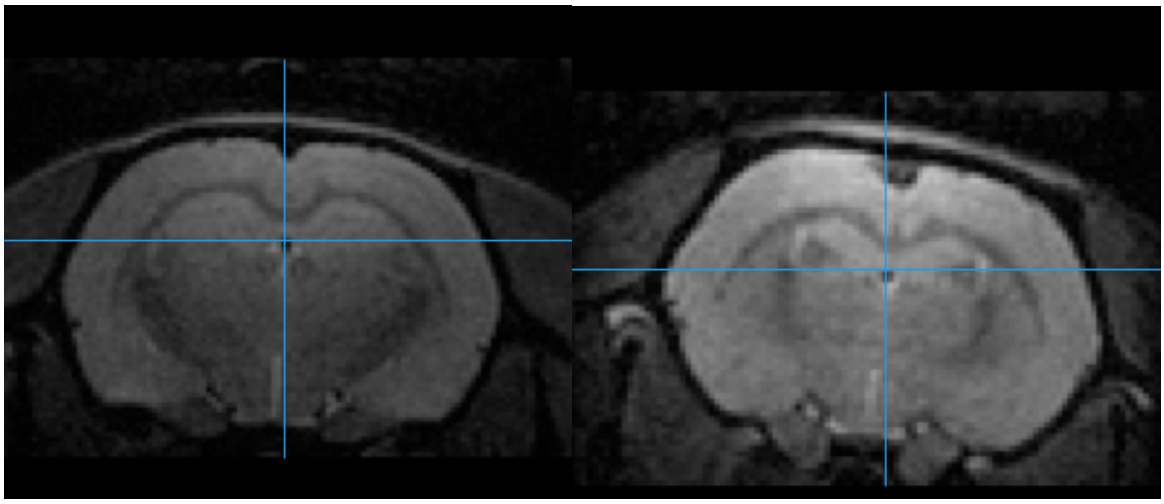

Figure 5-1 Proper (left) and improper (right) placement of earpins . Bad positioning may casuse rotation of the brain.

To avoid improper positioning always a pilot scan is performed, if necessary the position was manually corrected. Minimum break of 48h was kept between the scans of the same subject to avoid quick adaptation to the anesthesia.

5.2.4 Software

The analysis pipeline consisted of many steps, which made of different software. DTI analysis software are primarily designed for clinical use. Therefore, preclinical data requires the voxel dimension multiplication by a certain factor to ensure its usability in these

programs. By multiplying dimension values in the file header, desired size was achieved. Alternative approach would be to use SPM mouse toolbox (Sawiak et al., 2009), which instead of changing the file values adjusts the preprocessing parameters. SPM mouse supports only preprocessing of the data, thus first method was selected.

There are many ways to produce the mask of the brain. It could be created manually in MATLAB (mathworks) or by using imaging software. In the project two methods were tested, brain extraction tool from FSL package (Jenkinson et al., 2012) and mask tool from ExploreDTI (Leemans et al., 2009). They were giving quite similar results, however ExploreDTI resulted in slightly better shape of the mask.

Figure 5-2 Comparison of brain masks. Mask created by EXPLORE DTI (left), mask created by FSL (right).

5.2.5 Eddy Current correction

Eddy currents are introduced in EPI sequences. They are induced by gradient coils and may cause spatial distortions of the image (Ahn & Cho, 1991). Before performing any mathematical operation on the images, eddy current correction should be executed.

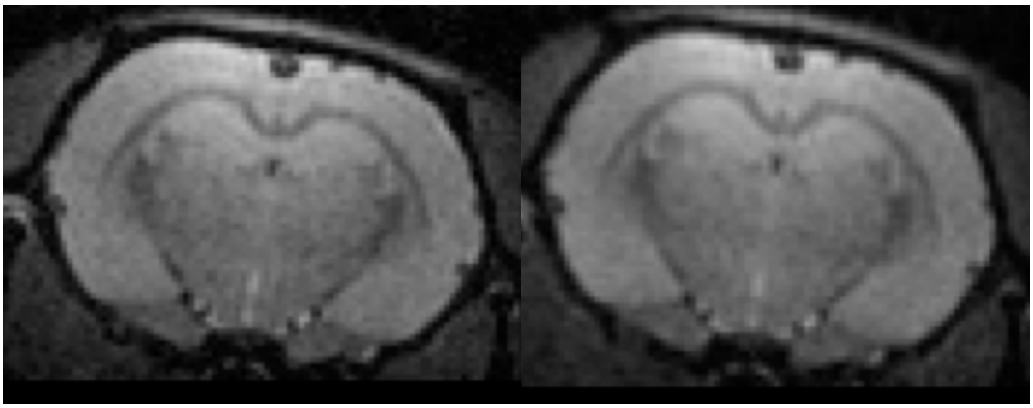

Figure 5-3 ECC correction. Eddy current correction makes the image smoother and increases the image contrast. Spatial distortions are minimized.

5.2.6 Tractography

Drawing a mask, which will be an origin for tracking, is very crucial and has to be done with great attention to avoid missing out of any details. Brains that were scanned differ and due to difficult positioning masks may vary. To decrease the differences, structures with easy to outline boundaries were chosen.

5.3 Discussion of results

The sequence that was used for TBI studies at the A.I Virtanen Institute was used as a reference for the project. The voxel size was 0.22 mm x 0.22 mm x 0.5 mm (Fig 4-1) With 14 slices that were acquired sequence did not cover the whole brain. The first step of optimization included increasing TR from 2000 ms to 4000 ms and number of slices from 14 to 30 (Fig 4-2). This ensured coverage of the whole brain. Ratio between TR and number of slices was kept at the same level in order to prevent overheating of the gradients. The olfactory bulb and cerebellum was discarded, as it was not of interest.

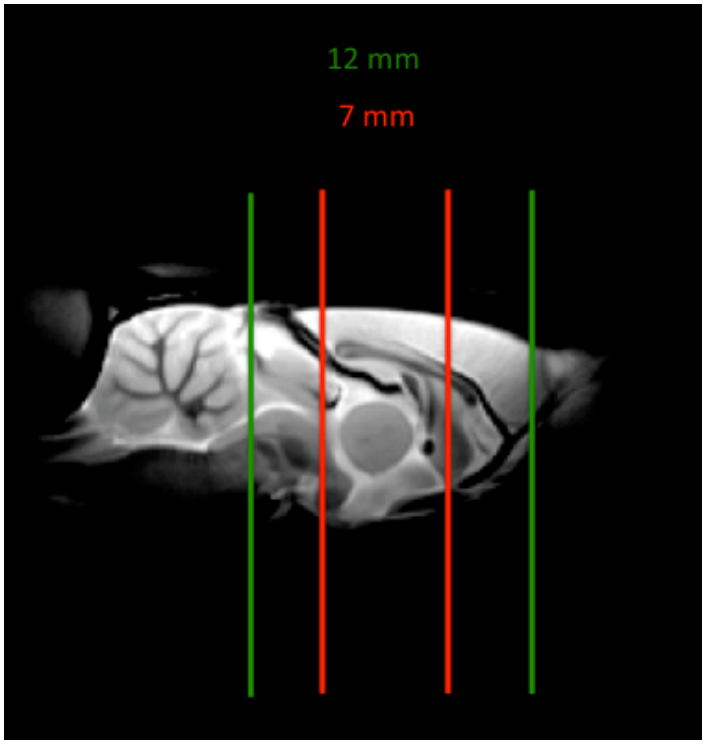

Figure 5-4 Effect of number of slices on brain coverage. Red lines show the area covered with 14 slices, while green lines shows tharea covered with 28 slices.

In Figure 4-4 and Figure 4-7 images with isotropic voxels are presented. They were acquired to check if selecting an image with isotropic voxels improves the results of fiber tracking. Acquiring an isotropic scheme ensures that averaging of fiber orientations is proper and it does not require more sophisticated modelling (Oouchi et al., 2012). This was primarily a reason for including 3D sequences in the protocol (Figure 4-10, Figure 4-11). Some spatial distortions are visible, however during that stage it was difficult to comprehend to what extent it will affect the final result. To further test the sequences we decided to keep the sequence that was commonly used (Fig 4-7), two with slightly higher resolution and variety of isotropic sequences (Figure 4-6, Figure 4-9). In Figure 4-12 B0 images with corresponding SNR values are presented. The sequence exhibited very poor SNR, therefore any improvement of the resolution should be examined in detail. It is possible to increase NEX and improve the quality but at the expense of scan time, which was already 2 h 8 min. To check if SNR ~ 20 allows a proper fitting of diffusion tensor, DEC maps were calculated. Another aim of this step was to examine if organization of the hippocampus is maintained. In Figure 4-16 it is easily seen that increasing the resolution, improves the projection of the hippocampus. To further evaluate the sequences probabilistic fiber tracking on anterior commissure is introduced (Figure 4-15). 3D sequences showed best results, unfortunately due

to magnetic field inhomogeneities images were spatially distorted and this discarded them from further evaluation.

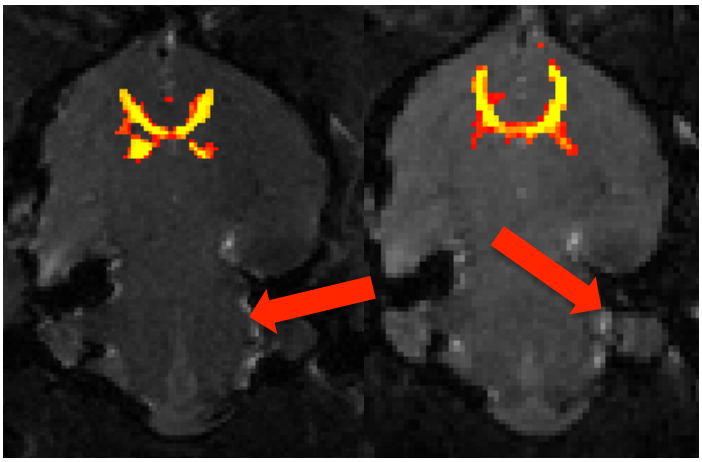

Figure 5-5 Magnetic Field inhomogenieties. Red lines show the area distorted due to magnetic field inhomogenetieis.

As shown in Figure 4-15 sequence with 0.22 mm x 0.22 mm x 0.5 mm resolution does not present as continuous tracts when compared to the two sequences with higher resolution. This is probably due to the fact that ST is more than 2 times higher than Vx and Vy. Some of the information is lost during tracking and it may have a crucial effect on the final result. Surprisingly 0.15 mm x 0.15 mm x 0.3 mm sequence which resulted in poor SNR (~13) gave promising tractography results. To further evaluate on tractographic reconstruction another structure for tracking was chosen. Corpus callosum shows high connectivity (Moseley et al., 2000); therefore it would be a proper structure to decide if poor SNR does not allow proper tractography.

As shown in Figure 4-18, sequence with higher resolution presents lower connectivity and not as many tracts are discovered. This may prove that SNR plays a crucial role for tractography experiments. Proper amount of signal is needed to allow appropriate performance of tractographic reconstruction.

5.4 Future work

5.4.1 Filtering

In the presented work pre-processing did not include any form of filtering. SNR can be improved by applying additional filters. As proven by Hecke et al. anisotropic filtering can be

applied on DTI data and possibly improve the results of tensor fitting. Anisotropic filtering smoothens the image according to its local features and takes under account the information about directionality. Method implemented in ExploreDTI (Jenkinson et al., 2012; Van Hecke et al., 2010) was applied to 0.15 mm x 0.15 m x 0.3 mm data. Tractography was performed on corpus callosum and results were compared.

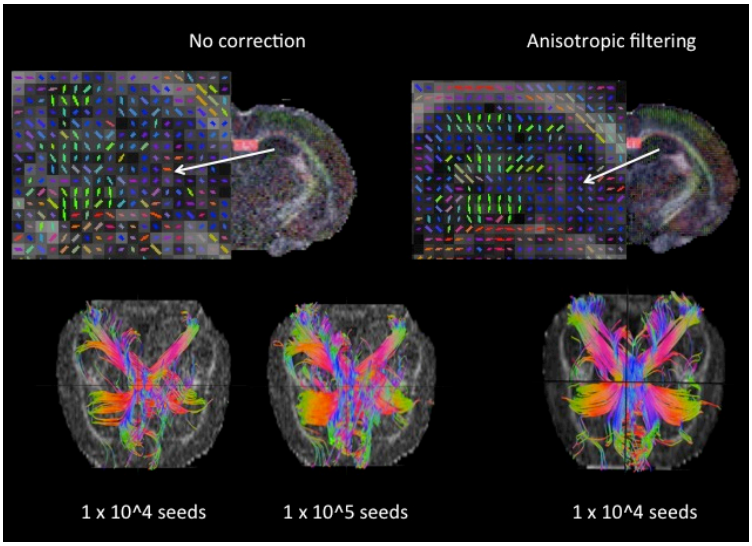

Figure 5-6 Effect of anisotropic filtering. Figure shows how organization of hippocampus benefits from the application of anisotropic filter.

Anisotropic filtering significantly improves the tractography results in our case; therefore it should be further investigated.

5.4.2 Connectivity analysis

Choosing a proper validation for tractography is another crucial step. In case of this work tracking was performed on two well-known structures and results were compared with previous work (Preti et al., 2001; Asanuma et al., 2008; Figini et al., 2015). To enhance the validation methods, connectivity between various structures can be an important step. A segmentation template (Rumple et al., 2013) can be registered to DTI data. Based on labelled regions tractography can be performed between two or more regions of interest. This would give an idea of how to quantify the results.

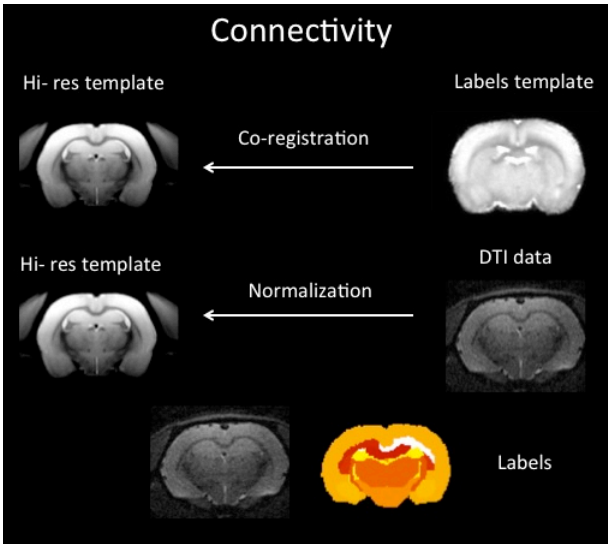

Figure 5-7 Registartion pipeline. Figure shows the procedure on how to register labelled template to existing DTI dataset.

A connectivity matrix could be calculated for each dataset and number of fibers could be examined.

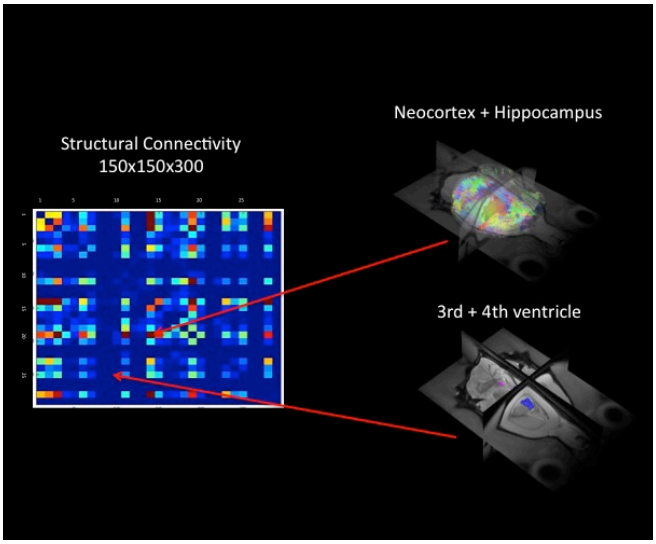

Figure 5-8 Connectivity analysis. After labelling of independent structures it is possible to perform tractography between desired regions and quantify obtained results.

5.5 Concluding remarks

The presented study introduces a processing pipeline for optimizing a voxel dimension in MR diffusion tensor imaging. As every MR system is different, this procedure could be used in variety of imaging facilities. The final sequence on our 7T scanner resulted in 0.2 mm x 0.2 mm x 0.4 mm voxel dimension, which in comparison with current approaches shows promising and competitive results (Asanuma et al., 2008; Seki et al., 2013; Figini et al., 2015). In vivo studies are limited by the scanning time and SNR. Therefore finding a DTI measurement sequence that provide great details and image quality is considered crucial in many applications, such as probabilistic tractography for brain connectivity research.

6 Appendix

6.1 MATLAB code

Bruk2FSL.m

```
[bvecs,bvals,dw] = nhpMpiBrukerBuildDiffusionGradients('method')
save('bvals','bvals','-ascii')
save('bvecs','bvecs','-ascii')

save('1.bval','bvals','-ascii')
save('1.bvec','bvecs','-ascii')
mkdir 01
!mv bvals ./01/bvals
!mv bvecs ./01/bvecs
!mv 1.bval ./01/1.bval
!mv 1.bvec ./01/1.bvec
DATA = aedes_readbruker('./pdata/1/2dseq');
SpRes = DATA.HDR.FileHeader.method.PVM_SpatResol*10;
THK = DATA.HDR.FileHeader.method.PVM_SliceThick*10;
done=aedes_write_nifti(DATA.FTDATA,'./01/raw_series.nii',...
                        'VoxelSize',[SpRes(1) SpRes(2) THK],'XYZUnits','mm');
vol = spm_vol('./01/raw_series.nii');
v = spm_read_vols(vol);
v1 = v(:,:,:,5);
v1=v1>mean(v1(:));
savenifti('nodif_brain_mask',v1,vol(1).mat,'int16');
!mv nodif_brain_mask.nii ./01/nodif_brain_mask.nii
!gzip ./01/nodif_brain_mask.nii
```

Bruk2FSL_3D.m

```
[bvecs,bvals,dw] = nhpMpiBrukerBuildDiffusionGradients('method')

save('bvals','bvals','-ascii')

new_bvec(1,:)=bvecs(2,:);

new_bvec(3,:)=bvecs(1,:);

new_bvec(2,:)=bvecs(3,:);

save('bvecs','new_bvec','-ascii')

mkdir 01

!mv bvals ./01/bvals

!mv bvecs ./01/bvecs

DATA = aedes_readbruker('./pdata/1/2dseq');

SpRes = DATA.HDR.FileHeader.method.PVM_SpatResol*10;

done=aedes_write_nifti(DATA.FTDATA,'./01/raw_series.nii',...

                        'VoxelSize',[SpRes(1) SpRes(2)
SpRes(3)],'XYZUnits','mm');

vol = spm_vol('./01/raw_series.nii');

v = spm_read_vols(vol);

v1 = v(:,:,:,5);

v1=v1>mean(v1(:));

savenifti('nodif_brain_mask',v1,vol(1).mat,'int16');

!mv nodif_brain_mask.nii ./01/nodif_brain_mask.nii

!gzip ./01/nodif_brain_mask.nii
```

dir_distribution.m

```
function  dir_distribution(bvecs_file)
```

```
vecs = load(bvecs_file);
sz = size(vecs);
figure;
X = vecs(1,:);
Y = vecs(2,:);
Z = vecs(3,:);
hold on
for ii = 1:sz(2)-1
plot3([X(1) X(ii+1)],[Y(1) Y(ii+1)],[Z(1) Z(ii+1)]);
end
for ij = 1:sz(2)-1
plot3([X(1) -X(ij+1)],[Y(1) -Y(ij+1)],[Z(1) -Z(ij+1)]);
end
[x,y,z]=sphere(20);
mesh(x,y,z,zeros(size(x)));
alpha(0.5);
axis image
```

V1_FA_map.m

```
clc
clear
!gunzip dti_V1.nii.gz
!gunzip dti_FA.nii.gz



FA = spm_vol('dti_FA.nii');
FA_vol = spm_read_vols(FA);
V1 = spm_vol('dti_V1.nii');
V1_vol = spm_read_vols(V1);
```

```
FA2=repmat(FA_vol,[1,1,1,3]);

V1_FA = V1_vol.*FA2;

savenifti('V1_FA',V1_FA,FA(1).mat,'float32');
```

6.2 Shell scripts

makefile (deterministic_tracking.sh)

```
DET_FILES := $(wildcard data/*/raw_series.nii)

SRC_FILES := $(addsuffix .src.gz, $(DET_FILES))

FIB_FILES := $(addsuffix .dti.fib.gz, $(SRC_FILES))

TRK_FILES := $(addsuffix .trk, $(FIB_FILES))

det_tracking: $(TRK_FILES)

@echo $(TRK_FILES)

.PRECIOUS: %/raw_series.nii.src.gz.dti.fib.gz

.PRECIOUS: %/b_table.txt

%/raw_series.nii.src.gz.dti.fib.gz.trk: %/raw_series.nii.src.gz.dti.fib.gz

/Applications/dsi_studio.app/Contents/MacOS/dsi_studio --action=trk --source=$<  -
-step_size=0.15 --fa_threshold=0.09 --min_length=10 --max_length=300 --
turning_angle=60 --seed_count=5000 --export=stat --output=$@

%/raw_series.nii.src.gz.dti.fib.gz: %/raw_series.nii.src.gz

/Applications/dsi_studio.app/Contents/MacOS/dsi_studio  --action=rec --source=$< -
-method=1

%/raw_series.nii.src.gz: %/file.nii

%/b_table.txt/Applications/dsi_studio.app/Contents/MacOS/dsi_studio --action=src -
-source=$< --b_table=$(<D)/b_table.txt --output=$@

%/file.nii: %/raw_series.nii

ln -s $(<F) $@

%/b_table.txt: %/bvals %/bvecs

python -c "import sys; print('\n'.join(' '.join(c) for c in zip(*(l.split() for l
in sys.stdin.readlines() if l.strip()))))" < $(<D)/bvals > bvals.txt

python -c "import sys; print('\n'.join(' '.join(c) for c in zip(*(l.split() for l
in sys.stdin.readlines() if l.strip()))))" < $(<D)/bvecs > bvecs.txt
```

```
paste -d" " bvals.txt bvecs.txt > $@

rm bvals.txt

rm bvecs.txt
```

makefile (probabilistic_tracking.sh)

```
# Makefile for running FSL probabilistic tractography

# author(s): Raimo Salo (raimo.salo@uef.fi)

# existing dti-series:

RAW_FILES := $(wildcard data/*/*/raw_series.nii.gz)

I_FILES := $(wildcard data/*/*/*dti_series.nii.gz)

# FA files to be produced:

O_FILES = $(subst dti_series.nii.gz,dti_res_,$(I_FILES))

all:

#############################################################################

# bedpostx

#############################################################################

# define file names

BEDPOSTX_FILES = $(subst dti_series.nii.gz,bedpostx,$(subst PAT_,,$(subst
CON_,,$(I_FILES))))

DATA_FILES = $(subst dti_series,data,$(subst PAT_,,$(subst CON_,,$(I_FILES))))

BVEC_FILES = $(subst .nii.gz,,$(subst data.,bvecs.,$(DATA_FILES)))

BVAL_FILES = $(subst .nii.gz,,$(subst data.,bvals.,$(DATA_FILES)))

NODIF_FILES = $(subst data.,nodif_brain_mask.,$(DATA_FILES))

# link to raw_series & XXX_nodif_BM with names required by bedpostx

%/data.nii.gz: %/raw_series.nii.gz

            -ln -s $(<F) $@

%/nodif_brain_mask.nii.gz: %/CON_nodif_brain_mask.nii.gz

            -ln -s $(<F) $@
```

```
%/nodif_brain_mask.nii.gz: %/PAT_nodif_brain_mask.nii.gz

	-ln -s $(<F) $@

# list of pre files bedpostx depends on

files: $(DATA_FILES) $(BVEC_FILES) $(BVAL_FILES) $(NODIF_FILES)

# bedpostx

bedpostx: files $(BEDPOSTX_FILES)

%/bedpostx: %/data.nii.gz %/nodif_brain_mask.nii.gz %/bvecs %/bvals

	bedpostx $(@D)

	touch $@

# probtrackx --mode=simple --seed=coords.txt --out=AC -l -c 0.2 -S 2000 --
steplength=0.5 -P 5000 --forcedir --opd -s
/home/raimos/data/JNK/data/WT1/01.bedpostX/./merged -m
/home/raimos/data/JNK/data/WT1/01.bedpostX/./nodif_brain_mask  --
dir=/home/raimos/data/JNK/data/WT1/01.bedpostX/./nodif_brain_mask

# /usr/share/fsl/4.1/bin/probtrackx --mode=simple --
seedref=/home/raimos/data/JNK/data/WT1/01.bedpostX/./nodif_brain_mask -o
nodif_brain_mask -x
/home/raimos/data/JNK/data/WT1/01.bedpostX/./nodif_brain_mask/fdt_coordinates.txt
-l -c 0.2 -S 2000 --steplength=0.5 -P 5000 --forcedir --opd -s
/home/raimos/data/JNK/data/WT1/01.bedpostX/./merged -m
/home/raimos/data/JNK/data/WT1/01.bedpostX/./nodif_brain_mask  --
dir=/home/raimos/data/JNK/data/WT1/01.bedpostX/./nodif_brain_mask



%/probtrackx: %/01/bedpostx

	mkdir --parents $(@D)/01.bedpostX/tracks

	probtrackx --seedref=$(@D)/01.bedpostX/nodif_brain_mask -o tracks --
seed=$(@D)/01.bedpostX/testmask  -l -c 0.2 -S 2000 --steplength=0.5 -P 5000 --
forcedir --opd -s $(@D)/01.bedpostX/merged -m $(@D)/01.bedpostX/nodif_brain_mask
--dir=$(@D)/01.bedpostX/tracks

#	probtrackx --mode=simple --seedref=$(@D)/01.bedpostX/nodif_brain_mask
-o tracks --seed=$(@D)/01.bedpostX/fdt_coordinates.txt  -l -c 0.2 -S 2000 --
steplength=0.5 -P 5000 --forcedir --opd -s $(@D)/01.bedpostX/merged -m
$(@D)/01.bedpostX/nodif_brain_mask  --dir=$(@D)/01.bedpostX/tracks

# view sample data

%/FSL: %/tracks_*

	fslview $(foreach tmp,$^,$(subst =, ,$(join $(tmp),=-l="Red-Yellow"=-
b=10,1000)))
```

```
#           echo $(subst =, ,$(join $^,=-l="Red-Yellow"=-b=10,1000))

################################################################################

# Create FA data using FDT

################################################################################

# shorthand target for fa images

.PHONY: fa_maps

fa_maps: $(O_FILES) run_lnk

# create FA images (+ some other)

#%dti_res_: %dti_series_ec.nii.gz %nodif_brain_mask_flld.nii.gz %bvecs %bvals

#           dtifit --data=$< --mask=$*nodif_brain_mask_flld.nii.gz --bvecs=$*bvecs
--bvals=$*bvals --out=$@$(subst /,_,$(*D))

%dti_res_: %dti_series_ec.nii.gz %nodif_brain.nii.gz %bvecs %bvals

            dtifit --data=$< --mask=$*nodif_brain_mask.nii.gz --bvecs=$*bvecs --
bvals=$*bvals --out=$@$(subst /,_,$(*D))

            touch $@ # phony file that tells whether results are up-to-date

# motion correction and eddy current correction - b0 + grad directions

%dti_series_ec.nii.gz: %dti_series.nii.gz

            TBSS/eddy_correct_rat $^ $@ 0

# brain mask

# fill holes in the brain masks

%nodif_brain_mask.nii.gz: %nodif_brain.nii.gz

echo $<

# 1) extract brain from b0 image using bet

# 2) create a brain mask

%nodif_brain.nii.gz: %nodif.nii.gz

            bet $< $@ -f .05 -m

# extract b0

%nodif.nii.gz: %dti_series.nii.gz
```

```
            fslroi $^ $@ 0 1

.PRECIOUS: %dti_series_ec.nii.gz %nodif.nii.gz %nodif_brain.nii.gz

################################################################################

# list data, check CON & PAT definitions

################################################################################

# make symbolic links with CON and PAT

.PHONY: run_lnk

run_lnk: data/lnk_data.sh data/lnk_bvecs.sh data/lnk_bvals.sh

            -sh data/lnk_data.sh

            -sh data/lnk_bvecs.sh

            -sh data/lnk_bvals.sh

data/lnk_bvals.sh: data/lnk_bvecs.sh

            cat $< | sed 's/bvecs/bvals/g' > $@

data/lnk_bvecs.sh: data/lnk_data.sh

cat $< | sed 's/raw_series\.nii\.gz/bvecs/; s/dti_series\.nii\.gz/bvecs/' > $@

data/lnk_data.sh: data/datalist.txt check_datalist

            cat $< | sed 's/\(.*\/\)\(.*.gz\)/ln -s \2 \1/; s/\t//;
s/$$/_dti_series.nii.gz/' > $@

# collect num of CON & PAT to design phase

WC_CON = $(shell grep -E '          CON$$' data/datalist.txt | wc -l)

WC_PAT = $(shell grep -E '          PAT$$' data/datalist.txt | wc -l)

# check that every line in the datalist has either CON or PAT definition

WC_ALL = $(shell cat data/datalist.txt | wc -l)

WC_CP = $(shell grep -E '           CON$$|      PAT$$' data/datalist.txt | wc -l)

.PHONY: err

ifneq ("$(wildcard data/datalist.txt)","")

ifeq '$(WC_ALL)' '$(WC_CP)'

CHECKED = CON PAT check ok
```

```
err: ;

else

CHECKED = 0

err: ; $(error Control and Patient groups not properly given in data/datalist.txt)

endif

else

CHECKED = 0

err: ; $(error Control and Patient groups not properly given in data/datalist.txt)

endif

.PHONY: check_datalist

check_datalist: data/datalist.txt err

            @echo $(CHECKED)

#           cat $< | wc -l

#           $(eval NUM := cat $< | wc -l)

#           echo $(NUM)

#           cat $< | grep -E '      CON|        PAT' | wc -l

# create the datalist from scratch

data/datalist.txt: $(RAW_FILES)

            echo $^ | sed 's/ /\n/g' > $@
```

7 References

Aedes; http://aedes.uef.fi

Ahn, C. B. and Z. H. Cho (1991). "Analysis of the eddy-current induced artifacts and the temporal compensation in nuclear magnetic resonance imaging." IEEE Trans Med Imaging 10(1): 47-52.

Asanuma, T., S. Doblas, Y. A. Tesiram, D. Saunders, R. Cranford, J. Pearson, A. Abbott, N. Smith and R. A. Towner (2008). "Diffusion tensor imaging and fiber tractography of C6 rat glioma." J Magn Reson Imaging 28(3): 566-573.

Baldwin, L. N., K. Wachowicz, S. D. Thomas, R. Rivest and B. G. Fallone (2007). "Characterization, prediction, and correction of geometric distortion in 3 T MR images." Med Phys 34(2): 388-399.

Basser, P. J. (1995). "Inferring microstructural features and the physiological state of tissues from diffusion-weighted images." NMR Biomed 8(7-8): 333-344.

Basser, P. J., S. Pajevic, C. Pierpaoli, J. Duda and A. Aldroubi (2000). "In vivo fiber tractography using DT-MRI data." Magn Reson Med 44(4): 625-632.

Blink, E. (2004). Basic MRI Physics.

Brown, R. W., Y.-C. N. Cheng, E. M. Haacke, M. R. Thompson and R. Venkatesan (2014). Magnetic resonance imaging : physical principles and sequence design. Hoboken, New Jersey, John Wiley & Sons, Inc.

Bruker; www.bruker.com.

Bushberg, J. T. (1994). The essential physics of medical imaging. Baltimore, Williams & Wilkins.

Einstein, A., R. Furth and A. D. Cowper (1926). Investigations on the theory of the Brownian movement. London,, Methuen & Co. ltd.

Ellingson, B. M., S. N. Kurpad and B. D. Schmit (2008). "Ex vivo diffusion tensor imaging and quantitative tractography of the rat spinal cord during long-term recovery from moderate spinal contusion." J Magn Reson Imaging 28(5): 1068-1079.

FDT; http://www.fmrib.ox.ac.uk/analysis/research/fdt/

Fields, R. D. (2008). "White matter matters." Sci Am 298(3): 42-49.

Figini, M., I. Zucca, D. Aquino, P. Pennacchio, S. Nava, A. Di Marzio, M. G. Preti, G. Baselli, R. Spreafico and C. Frassoni (2015). "In vivo DTI tractography of the rat brain: an atlas of the main tracts in Paxinos space with histological comparison." Magn Reson Imaging 33(3): 296-303.

Gulani, V., A. G. Webb, I. D. Duncan and P. C. Lauterbur (2001). "Apparent diffusion tensor measurements in myelin-deficient rat spinal cords." Magn Reson Med 45(2): 191-195.

Guy, C. and D. Ffytche (2005). An introduction to the principles of medical imaging. LondonSingapore ; Hackensack, NJ, Imperial College Press ; Distributed by World Scientific Pub.

Jenkinson, M., C. F. Beckmann, T. E. Behrens, M. W. Woolrich and S. M. Smith (2012). "Fsl." Neuroimage 62(2): 782-790.

Jezzard, P. (2012). "Correction of geometric distortion in fMRI data." Neuroimage 62(2): 648-651.

Jirsa, V. K. and A. R. McIntosh (2007). Handbook of brain connectivity. Berlin ; New York, Springer.

Jones, D. K. (2010). Diffusion MRI : theory, methods, and application. Oxford ; New York, Oxford University Press.

Jones, D. K. and P. J. Basser (2004). ""Squashing peanuts and smashing pumpkins": how noise distorts diffusion-weighted MR data." Magn Reson Med 52(5): 979-993.

Kalthoff, D., J. U. Seehafer, C. Po, D. Wiedermann and M. Hoehn (2011). "Functional connectivity in the rat at 11.7T: Impact of physiological noise in resting state fMRI." Neuroimage 54(4): 2828-2839.

Le Bihan, D., E. Breton, D. Lallemand, P. Grenier, E. Cabanis and M. Laval-Jeantet (1986). "MR imaging of intravoxel incoherent motions: application to diffusion and perfusion in neurologic disorders." Radiology 161(2): 401-407.

Leemans, A. J., B.; Sijbers, J.;Jones, DK. (2009). ExploreDTI: a graphical toolbox for processing, analyzing, and visualizing diffusion MR data. 17th Annual Meeting of Intl Soc Mag Reson Med. Hawaii, USA

MATLAB "http://www.mathworks.com."

McRobbie, D. W. (2007). MRI from picture to proton. Cambridge, UK ; New York, Cambridge University Press.

Meynert, T. (1968). Psychiatry; a clinical treatise on diseases of the fore-brain based upon a study of its structure, functions, and nutrition. Part I. New York,, Hafner Pub. Co.

Mori, S. and J. D. Tournier (2014). Introduction to diffusion tensor imaging and higher order models. Amsterdam ; Boston, Elsevier/Academic Press.

Mörters, P., Y. Peres, O. Schramm and W. Werner (2010). Brownian motion. Cambridge, UK ; New York, Cambridge University Press.

Neurolex.org; http://neurolex.org/wiki/

Nicholls, J. G. (2012). From neuron to brain. Sunderland, Mass., Sinauer Associates.

Oouchi, H., K. Yamada, K. Sakai, O. Kizu, T. Kubota, H. Ito and T. Nishimura (2007). "Diffusion anisotropy measurement of brain white matter is affected by voxel size: underestimation occurs in areas with crossing fibers." AJNR Am J Neuroradiol 28(6): 1102-1106.

Preti, M. G., A. Di Marzio, A. Mastropietro, D. Aquino, G. Baselli, M. M. Lagana, I. Zucca, C. Frassoni and R. Spreafico (2011). "Tractographic reconstruction protocol optimization in the rat brain in-vivo: towards a normal atlas." Conf Proc IEEE Eng Med Biol Soc 2011: 8467-8470.

Rumple, A., M. McMurray, J. Johns, J. Lauder, P. Makam, M. Radcliffe and I. Oguz (2013). "3-dimensional diffusion tensor imaging (DTI) atlas of the rat brain." PLoS One 8(7): e67334.

Sawiak, SJ.; Williams, GB.; Wood, NI; Morton, AJ.; Carpenter, TA. (2009). SPMMouse: a new toolbox for SPM in the animal brain. 17th Annual Meeting of Intl Soc Mag Reson Med. Hawaii, USA

Seki, F., K. Hikishima, S. Nambu, K. Okanoya, H. J. Okano, E. Sasaki, K. Miura and H. Okano (2013). "Multidimensional MRI-CT atlas of the naked mole-rat brain (Heterocephalus glaber)." Front Neuroanat 7: 45.

Skare, S., M. Hedehus, M. E. Moseley and T. Q. Li (2000). "Condition number as a measure of noise performance of diffusion tensor data acquisition schemes with MRI." J Magn Reson 147(2): 340-352.

Skare, S., T. Li, B. Nordell and M. Ingvar (2000). "Noise considerations in the determination of diffusion tensor anisotropy." Magn Reson Imaging 18(6): 659-669.

Taylor, W. D., E. Hsu, K. R. Krishnan and J. R. MacFall (2004). "Diffusion tensor imaging: background, potential, and utility in psychiatric research." Biol Psychiatry 55(3): 201-207.

Thibodeau, G. A. and K. T. Patton (1997). Structure & function of the body. St. Louis, Mosby Year Book.

Van Hecke, W., A. Leemans, S. De Backer, B. Jeurissen, P. M. Parizel and J. Sijbers (2010). "Comparing isotropic and anisotropic smoothing for voxel-based DTI analyses: A simulation study." Hum Brain Mapp 31(1): 98-114.

Westbrook, C. and C. Kaut (1998). MRI in practice. Oxford England ; Malden, MA, USA, Blackwell Science.

Yeh, F. C., T. D. Verstynen, Y. Wang, J. C. Fernandez-Miranda and W. Y. Tseng (2013). "Deterministic diffusion fiber tracking improved by quantitative anisotropy." PLoS One 8(11): e80713.